T.C
YEDITEPE UNIVERSITY
INSTITUTE OF HEALTH SCIENCES
DEPARTMENT OF HEALTH PHYSICS

DIRECT CALCULATION AND MONTE CARLO SIMULATION COMPARISON OF IMAGE QUALITY PARAMETERS ACQUIRED BY DIFFERENT GAMMA CAMERA COLLIMATORS

MASTER THESIS

BURAK AKGÜL

İstanbul , 2022

T.C
YEDITEPE UNIVERSITY
INSTITUTE OF HEALTH SCIENCES
DEPARTMENT OF HEALTH PHYSICS

DIRECT CALCULATION AND MONTE CARLO SIMULATION COMPARISON OF IMAGE QUALITY PARAMETERS ACQUIRED BY DIFFERENT GAMMA CAMERA COLLIMATORS

MASTER THESIS

BURAK AKGÜL

SUPERVISOR
Prof. Dr. Ş. İpek KARAASLAN

CO-ADVISOR
DR. TÜRKAY TOKLU

İstanbul , 2022

THESIS APPROVAL FORM

Institute : Yeditepe University Institute of Health Sciences

Programme : Sağlık Fiziği

Title of the Thesis : Direct Calculation and Monte Carlo Sımulation Comparison of Image Quality Parameters Acquıred by Different Gamma Camera Collimators

Owner of the Thesis : Burak Akgül

Examination Date : 23.09.2022

This study have approved as a Master Thesis in regard to content and quality by the Jury.

	Title, Name-Surname (Institution)
Chair of the Jury:	Prof. Dr. Zuhal Er (İSTANBUL TEKNİK ÜNİVERSİTESİ)
Supervisor:	Prof.Dr. Şerife İpek KARAASLAN (YEDİTEPE ÜNİVERSİTESİ)
Co-advisor	Dr. Türkay TOKLU (YEDİTEPE ÜNİVERSİTESİ İHTİSAS HASTANESİ)
Member/Examiner:	Prof. Dr. Nesrin ALTINSOY (İSTANBUL TEKNİK ÜNİVERSİTESİ)
Member/Examiner:	Prof. Dr. Nalan ALAN SELÇUK (YEDİTEPE ÜNİVERSİTESİ İHTİSAS HASTANESİ)

APPROVAL

This study has been approved by the jury regarding with the related articles of Yeditepe University Graduate Education and Examinations Regulation and has been approved by Administrative Board of Institute with decision dated ..... and numbered .....

Prof. Dr. Bayram Yılmaz

Director of Institute of Health Sciences

DECLARATION

I hereby declare that this work is my own, that there is no ethical situation in the planning, creation, writing and any other step, that I provide all the information in the study in accordance with the academic and ethical rules, that all information and comments not obtained by this study are provided by the source, and that I specify these resources in the resource list, and that I have not acted in violation of patent and copyright during writing of this study.

Date

Signature

Burak Akgül

ACKNOWLEDGEMENT

In my thesis, I would like to thank Yeditepe University Vice Rector Prof. Dr. S.İpek KARAASLAN, Yeditepe University Faculty of Medicine, Head of Nuclear Medicine Department Prof. Dr. Nalan ALAN SELÇUK and Yeditepe University Lecturer Dr. To Türkay TOKLU,

To Yeditepe University Hospital Nuclear Medicine Department employees who always make me feel at home in my department,

To my mother Kadriye AKGÜL, my father Muhteşem AKGÜL and my sister Burçin AKGÜL, for whom I am grateful for their presence in every step I have taken in life until today,

To my dear wife Emine AKGÜL, with whom I share this life together and whom I know I cannot reach today, and to my son Yekta Ege AKGÜL, the reason I live.

My deepest love and thanks.

TABLE OF CONTENTS

LIST OF TABLES

LIST OF FIGURES

LIST OF ABBREVIATIONS

2D	Two Dimensions
3D	Three Dimensions
cc	Cubic Dentimeter
CFOV	Central Field of View
cps	Count Per Second
CT	Computed Tomography
eV	Electron Volt
FBP	Filtered Back Projection
FDG	Fluorodeoxyglucose
FOV	Field of View
FWHM	Full Width Half Maximum
FWTM	Full Width at Tenth Maximum
Ga-67	Gallium 67
GHz	Giga Hertz
GP	General Purpose
HE	High Energy
HR	High Resolution
I-123	Iodine 123
I-131	Iodine 131
In-111	Indium 111
kcps	Kilo Count Per Second
KeV	Kilo electron volt
LEAP	Low Energy All Purpose
LEGP	Low Energy General Purpose
LEHR	Low Energy High Resolution
LEHRS	Low Energy High Resolution Sensitivity
LEHS	Low Energy High Sensitivity
LET	Linear Energy Transfer
MBq	Mega Becquerel
MC	Monte Carlo
mCi	Millicurie

ME	Medium Energy
ml	Milliliters
MR	Magnetic Resonance
MRI	Magnetic Resonance Imaging
NaI	Sodium Iodide
NEMA	National Electrical Manufacturers Association
PET	Positron Emission Tomography
PHA	Pulse Height Analysis
PMT	Photo Multiplier Tube
ROI	Region of interest
RTP	Radio Therapy Planning
SPECT	Single Photon Emission Computed Tomography
SVS	System Volume Sensitivity
Tc-99m	Technetium-99m
UFOV	Useful Field of View
US	Ultrasound
VSAC	Volume Sensitivity per Axial Centimeter
Z	Atomic number

ABSTRACT

Akgül, B. (2022). Direct Calculation and Monte Carlo Simulation Comparison of Image Quality Parameters Acquired by Different Gamma Camera Collimators. Yeditepe University, Institute of Health Science, Department of Medical Physics MSc thesis, İstanbul.

This thesis aims to investigate National Electrical Manufactures Association (NEMA) performance measurements for Low Energy High Resolution (LEHR) and new developed Low Energy High Resolution Sensitivity (LEHRS) collimators and also simulate same measurements with Monte Carlo platform. Measurements done with the GE Discovery 670 SPECTCT installed in Yeditepe University Koşuyolu Hospital.

Also, a Monte Carlo simulation software GATE used for simulations. Both LEHR and LEHRS collimators were represented with a gamma camera setup in GATE software for measurements.

During the GATE simulations, Gamma Camera, crystals and collimators were investigated to simulate. After those setups at GATE pre-defined NEMA measurements were run to simulate, and results collected. As last step pre-defined NEMA measurements were run on gamma camera installed in Yeditepe University Hospital to compare the results.

Keywords: NEMA, Monte Carlo, GATE, Geant, Gamma camera, Collimator

ÖZET

Akgül, B. (2022). Gama Kameralardaki Farkli Kolimatörlerden Elde Edilen Görüntü Kalitesi Parametrelerinin Doğrudan Ölçüm ve Monte Karlo Simülasyon Yöntemiyle Karşilaştirilmasi. Yeditepe Üniversitesi Sağlık Bilimleri Enstitüsü, Sağlık Fiziği ABD., Yüksek Lisans Tezi. İstanbul.

Bu tezin amacı, Gama Kameralarda kullanılan Düşük Nerjili Yüksek Çözünürlüklü ve yeni üretilen Düşük Enerjili Yüksek Çözünürlük ve Hassasiyetli kolimatörlerin NEMA ölçümlerinin yapılması ve aynı ölçümlerin Monte Carlo simülasyon ortamında yapılarak sonuçların kıyaslanmasıdır. Ölçümler Istanbul Yeditepe Üniversitesi Koşuyolu Hastanesi'nde kurulu olan GE Marka Discovery 670 cihazı ile yapılmıştır.

Aynı zamanda bir Monte Carlo simülasyon platformu olan GATE kullanılarak yapılan ölçümler simülasyon ortamında tekrarlanmıştır.

Simülasyon işlemlerinde Gama kamera, kristal, kolimatörler ve gama kamera bileşenleri simülasyon için Gate platformunda tasarlandı. Bu adımlardan sonra Gate platformunda bulunan NEMA ölçümleri çalıştırıldı ve sonuçlar toplanarak kaydedildi. Son adımda aynı testler Gama Kameralarda fiziksel olarak yapıldı ve sonuçlar kaydedildi.

Anahtar kelimeler: NEMA, Monte Carlo, GATE, Geant, Gamma camera, Collimator

1. INTRODUCTION & PURPOSE

Gamma cameras are medical imaging systems developed in the1950s by Hal Anger. These scanners also known as scintillation systems became the main imaging systems in Nuclear Medicine. The large detector surface of gamma cameras gives the opportunity to scan different parts of the body including bones, kidneys, heart, brain, and lungs.

Like every medical imaging scanner, working under the highest performance give the ideal image quality in gamma cameras. To get the best image quality from a scanner, several tests and calibrations should be done for medical imaging scanners.

In North America, the National Electrical Manufacturers Association (NEMA) is the organization setting the standards used on behalf of various electrical equipment classes and medical imaging products. The organization was established to make products and machines safer, more reliable, and more efficient. NEMA has seven core markets it addresses, from industrial products to transportation systems, with the ultimate goal of developing performance standards.

The NEMA performance criteria supply the only defined and repeatable measures of scintillation-camera efficiency being universally acknowledged by producers. The tests need a way to differentiate other than an established good computer, according to the NEMA document explaining the quality requirements.

To ensure that a medical imaging scanner is operating in the best possible way, it is crucial for the scanner to pass NEMA performance analysis. To ensure the safety of patients, medical imaging machines must operate at their optimum performance, and the radiation dose that must be supplied to or received by patients must be closely supervised.

The findings of testing carried out in accordance with NEMA rules enable simple camera effectiveness monitoring and reporting, system comparison, and/or development of uniform QC processes. (1)

Practical applications for NEMA traceable measurements include normal quality control and end-user scintillation camera acceptance testing. (2)

Monte Carlo (MC) simulation is a kind of computerized mathematical technique enabling individuals to explain risk in quantitative analysis and making decisions. The technique is utilized by professionals in such common disparate areas as finance, energy, managing project production, engineering, oil & gas, transportation, research and development, environment, and insurance.

The Open Gate collaboration created the Monte Carlo simulation platform known as GATE. GATE combines unique characteristics related to emission tomography with the pros of the GEANT4 simulation toolbox which involves well-validated physics models, geometry definitions widely used, and strong visualization and 3D rendering tools.

The available medical scanners can be simulated with Gate platform such as gamma cameras, positron emission tomography (PET), computed tomography (CT), or radiotherapy systems.

The depiction of timing-dependent events, including source or detector mobility and source decay dynamics, is specifically permitted by GATE. With the help of this feature, it is possible to examine dynamic reconstruction techniques and recreate time curves under exact acquisition situations (3)

Gate Monte Carlo simulation also opens new doors to design medical scanner parts in a different way, helps scientists design new imaging technics, and develops new methods. (4)

The subject of this desertion is to measure NEMA performance tests of the Gamma Camera and simulate the same measurements on GATE Monte Carlo simulation to compare the results.

2. GENERAL INFORMATION

2.1. Types of Medical Imaging

The phrase "medical imaging" refers to a variety of technological developments being used to seek the human body with the aim of diagnosing, tracking, or treating medical problems. Every kind of device delivers unique information on the bodily area being investigated or healed, in relation to any potential infection, harm, or the efficiency of medical care.

Medical imaging comprises all diagnostic and curative examinations and medical interventions in an ordinary radiology department. It includes multiple imagery methods and processes to see the physical species for treatment, clinical, and post-treatment functions. It is fundamental to attempt to improve the public's health among all age categories. Including:

- X-ray imaging (involving example plain x-rays, fluoroscopy)
- Magnetic resonance imaging (MRI)
- Ultrasound (US)
- Computed tomography (CT)
- Nuclear Medicine: inter radioisotopes screening, for instance besides "classical" scintigraphy, such as bone scans, PET is recognized as a unique approach.
- Hybrid imaging

Medical imaging, specifically X-ray-based studies, and ultrasonography, is vital in a range of medical scenarios and at every main stage of health care. Accurate diagnoses in rehabilitative and pain management, public health, and preventive medicine are required for making informed choices. Even if medical/clinical judgment might be competent prior to care for a number of diseases, trying some medical diagnostic services is key in assuring, correctly diagnosing, and charting the courses of many ailments and also in monitoring replies to treatment.

Imaging is a precious source to heal diseases and significant part of therapists when used adequately.

Knowing when imaging is necessary is crucial since doing so wastes money and raises the risk of having surgery before it is necessary.

The inherent merits of the combination imaging modalities are frequently

synergistically blended to develop a novel and more efficient modality. Current hybrid imaging techniques include;

- PET-CT
- SPECT-CT
- MRI-PET
- MRI-SPECT
- Ultrasound and MRI
- Ultrasound and CT
- MRI and CT

One step closer to specific therapy, greater diagnostic value, and sensitive indicators of invasive procedures are really only a few of the added benefits of hybrid imagery.

The improved capacity of medical research and the discovery of various drugs have been advantageous to humankind and the overall world. The profession of surgery has profited greatly from scientific discovery too. Nevertheless, the first prerequisite previous to therapy is the precise and exact identification of disorders. Proper diagnosis will be achievable when bio-instruments become ever more advanced. The use of medical graphics in training, diagnostic testing, and treatments by doctors is crucial. With the aid of X-ray CT and MR imaging, imaging methods are frequently thought of as a method to represent structures within the body. Yet, it generally serves physiologic function rather than morphology better. Medical imaging has had made a tremendous influence on the healthcare industry with the advancement of electronic and image innovation. Medical image processing has become a hot topic since the reliability of medical imaging affects diagnosis, and clinical applications that want to save and retrieve images for later use demand some viable solution to store such pictures in detail. (5)

2.1.1. Nuclear Medicine Imaging (NM & NMCT)

Nuclear medicine is a subspecialty of radiology using minimal amounts of radioisotopes, known as radiopharmaceuticals, to investigate the structure and functioning of systems. Nuclear medicine imaging includes a number of different academic disciplines. These include chemistry, biology, physics, arithmetic, and computer science. In this field of imaging, irregularities that initially exhibit themselves very early in the development of a disorder, such as thyroid cancer, are typically found

and managed.

Any nuclear medicine imaging investigation may generally be split into two categories: (a) single-photon imaging, which analyzes photons directly released from radioactive nuclei; and (b) coincidence imaging, which measures pairs of 511-keV photons that are absorbed within absolutely opposite directions. (6)

Following the positron annihilation of the examined nuclei, positron annihilation produces these photons. Single-photon imaging examinations employ Anger cameras with detectors, whereas PET studies use cameras with many tiny detectors arrayed in various rings around the patient. These instruments are sometimes referred to as "SPECT cameras" since almost all available at the moment Anger cameras can rotate and reconstruct tomographic SPECT images.

Because X-rays pass through soft tissue structures like the bowels, lungs, and vasculature, they are difficult to notice on a typical X-ray without the usage of a contrast agent. As a result, the tissue may now be seen even certainly. Nuclear imaging enables the assessment of the nature and action of tissues and organs. The level of a radiopharmaceutical that is taken, or "absorbed," by the organ or tissue, under study may reveal the degree of function of that organ or tissue. Therefore, the significant aim of diagnostic X-rays is to check the anatomy. Nuclear imaging is used to assess how organs and tissues perform.

A very low dose of radioactive material is administered throughout the technique to simplify the investigation. Radioactive isotopes, also known as a radionuclide, is incorporated by body tissue (radiopharmaceutical or radioactive tracer). Radionuclides come in a wide range. These include diverse aspects of the elements iodine, xenon, technetium, thallium, and gallium. A specific radionuclide will be used according to the type of study and the body part being probed.

The right choice of a radioactive tracer (radiopharmaceutical) is essential for successful nuclear medicine imaging. A radioactive substance is made up of radioactive isotope molecules joined to pharmaceutical molecules; both constituents must be adapted for the job at hand. The component releases gamma photons, which have a power high enough for a substantial number of radiation to leave the body but a low enough energy to be blocked by the detectors. Moreover, the radioisotope has to be generally simple to make, convenient to connect to pharmaceuticals, and have a half-life that is both long enough for handling and brief sufficient to stay too long in a person's body (7).

Following the radionuclide is delivered and placed in the body tissue under

observation, radiation will be emitted. This radiation is found using a radiation detector. The most widely used type of detector is the gamma camera. A computer produces and stores digital signals when the radiation is identified by the gamma camera.

One or more Sodium Iodide (NaI) scintillation detectors circle around a patient in a traditional SPECT system to gather data on the two-dimensional dispersion of the detected photons (growth figures) from various angles. A conventional detector has a width of 3/8 inches and is around 40 cm by 50 cm. These detectors are mounted above a gantry, which formerly featured so-called "closed gantry" layouts more frequently before evolving to more "open" arrangements (8).

By evaluating the radionuclide's activities well within the body during a nuclear examination, a healthcare professional can investigate and determine a variety of scenarios, including malignancies, infections, hematomas, organ expansion, and cysts. You may assess blood flow and organ performance using nuclear imaging.

The places where the radionuclide concentrates more abundantly are alluded to as "hot spots." The places which do not uptake the radionuclide and seem less spectacular on the scan pictures are described as being "cold spots."

For the period of planar imaging, the gamma camera is motionless. What is obtained are visuals in two dimensions (2D). Computed tomography with single photon tomography, or SPECT, yields axial "pieces" of the part of the body since the gamma camera circles around the patient. These scars look like those formed by a CT scan. In some cases, like PET scans, the SPECT data can be used to produce three-dimensional (3D) visuals. Scanners are used to diagnose a broad range of illnesses and medical problems. Here are a few of the most common methods:

- Renal screenings are used to assess the kidneys and determine any defects. These include diminished renal function or a stoppage of the renal blood flow.
- Thyroid; they help to more properly examine immune function or hypothyroidism or abnormalities.
- Bone; they are used to identify abnormalities and other ailments of the skeletons, to detect any degenerative or progressive changes in the joints, and/or to figure out the root of any bone ache or aggravation.
- Gallium is used to detect cancer, abscesses, and actively spreading viral and/or autoimmune conditions.
- Cardiograms, which are used to evaluate the function of the heart, determine the

degree of heart muscle injuries following a myocardial infarction, and reveal abnormal circulation of blood to the heart.

- Brain; they are used to examine problems regarding the brain or the blood vessels to the left hemisphere.
- Breast; to diagnose breast diseased tumors, mammograms and these are generally used in combination.

As was already noted, a range of body parts and tissues can be inspected using nuclear medicine. Each type of scan uses distinct tools, radionuclides, and methods (10).

Tracer (radionuclide) administration, image capture, and image analysis make up a nuclear medicine scan. A few seconds to many days may pass between the delivery of the tracer and the capture of the photographs. Depending on the body tissue being investigated and the tracer being used, the time will vary. While some scans can be finished in a matter of minutes, others could require the patient to come back numerous times over the course of several days.

The use of nuclear medical techniques has, more significantly, significantly increased patient care in numerous ways. Medical information that might normally be missing or need more invasive methods, such as surgery or biopsy, may now be obtained by doctors more effectively because of nuclear imaging. When combining Positron Emission Tomography (PET) imaging with surgery to detect if ambiguous lung lesions shown on CT are malignant, in particular, it has been projected to save over $400,000 per 100 patients (9)

2.1.2 Positron Emission Tomography (PET)

PET relies on the simultaneous annihilation of a positron and an electron, which creates multiple co-linear (511-keV) beams that are roughly 180 degrees separated. The aggregate count rate of independent annihilation particles is known as the "singles count rate," and annihilation particle is detected by a detector, it is referred to as a "single" occasion.

A "true coincidence event" (referred to simply as "true") is formed when both photons from an annihilation are captured concurrently (in coincidence) in diametrically opposed detectors (10).

Nuclear medicine processes and steps such as (PET) observe the metabolic activity of the cells in various body tissues. Actually, PET connects nuclear medicine to

biochemical analysis. PET helps the visualization of biochemical changes that occur in the human body, including the metabolism of the heart muscle (the duration by which cells alter food into energy after food digestion and being underlined the circulation). PET is commonly tried in patients with cancer, brain, heart, or disorders.

PET is distinct from various nuclear medicine tests in which it assesses metabolism inside human tissues, whereas other tests measure the concentration of radioactive material in a particular area of body tissue to assess that tissue's function.

Due to the fact that PET is a nuclear medicine procedure, a radiopharmaceutical also known as a radionuclide or radioactive tracer is utilized as a small amount of radioactivity to aid in the analysis of the tissue being studied. Specifically PET investigations not only measure the function of an organ or tissue but also evaluate the physiology, architecture (structure), and biochemical characteristics. As a result, PET may be able to identify the beginning of a disease process in an organ or tissue before other imaging procedures like CT or MRI can find out structural alterations associated with the disease (MRI).

The principal proposed PET application of the first line of clinical PET/CT scanners, notably 18F-FDG whole body surveys, had a substantial impact on the design of these systems. Currently, nearly 90% of all clinical PET examinations are connected to oncology.

Large diameter, fast response, and strong spatial resolution are desirable qualities of the PET component.

For radiation treatment planning (RTP) usage, a large patient port (70 cm in diameter is conventional for CT) is required since these patients commonly need to be accurately positioned utilizing big devices such as dedicated head and arm holds. The patient must not be moved during the co-scan if the range is 100 cm or more on both the PET and the CT (11).

The doctors and scientists most likely to use PET include cardiologists, neurologists, and neurosurgeons (doctors who focus on treating and executing on illnesses of the brain and nervous system) (by doctors who are specialized in the heart treatment). But as PET technology improves, that method begins to be utilized in a more regular way in other professions PET may also be used in combination with other diagnostic tools like computed tomography (CT) or magnetic resonance imagery to offer more comprehensive information about malignant (cancerous) tumors and other abnormalities (MRI). A more recent invention that merges PET and CT technologies is the PET/CT scanner. PET/CT

has great power for detecting illness and management of lung cancer and also the investigation of epilepsy, Alzheimer's disease, and coronary artery disease.

PET operations were initially only executed in dedicated PET facilities due to the necessity that a radiochemistry lab and cyclotron, in addition to a PET scanner, be available for the manufacturing of radiopharmaceuticals. All that is essential to do a PET scan these days is a scanner due to the widespread production and delivery of radiopharmaceuticals to PET labs.

Gamma camera systems, a method, that will enhance the accessibility of PET imaging (devices for scanning patients injected with small amounts of radionuclides and for the time being in application with other nuclear medicine processes). These applications are updated to apply PET scan investigations. The gamma camera system may accomplish a scan faster and with less money than a conventional PET scan.

Generally speaking, organs and/or tissues may be evaluated utilizing PET scans to ascertain the presence of illness or other disorders. Additionally, the functioning of an organ, such as the brain or the heart may be investigated using PET. The most common uses of PET are for the diagnosis of cancer.

The following, among other things, are more specific causes for PET scans:

- To evaluate neurological illnesses including Alzheimer's disease and other kinds of dementia (conditions that cause a decline in mental function)
- Parkinson's disease. a neurological disorder marked by a little tremor, muscular weakness, and an odd gait that gets worse with time.
- Huntington's syndrome. a neurological disease that leads to gradual dementia, abnormal involuntary movements, and abnormal position and runs in families.
- Epilepsy. A neurological disorder characterized by repeated seizures. Neurovascular accident (stroke)
- To pinpoint the exact surgical location before undergoing brain surgery.
- To examine the brain following injury to look for bleeding, hematomas (blood clots), or perfusion (the flow of blood and oxygen) of the brain tissue.
- To diagnose cancer that spreads from the primary location of cancer to other areas of the body.
- To find the efficacy of treatments of cancer
- To assess the myocardial perfusion as a tool for evaluating the efficacy of a therapeutic technique to increase myocardial perfusion.

- To more precisely pinpoint lung lesions or tumors shown on chest CT or X-ray images
- By staging lesions and monitoring their development after therapy, staging lesions can help in the management and healing of lung cancer.
- To identify tumor recurrence earlier than with conventional diagnostic techniques (12).

2.2. Gamma Camera & Principles of Gamma Camera Imaging

The technical components that constitute the gamma camera, an instrument for sensing medical rays, each have a specific role to play in the process of photon observation. (13) It is impossible to go into considerable depth in this chapter on the respective functions of each of these components. The primary components of image acquisition are outlined in relation to their relative role in picture output. This list generally includes a collimator, crystal, PMT, preamplifier, amplifier, pulse height analyzer (PHA), position electronics, host computer for image analysis and data purification, and mainly a monitor for picture display. In a nutshell, after the patient has received the administration and is prepared for imaging, the incident photons first come into contact with the collimator. (13)

The hardware's role in creating the scatter of activity across various organs is handled by the collimator, which detects the directionality of incident radiation. Afterward, the approved particles interact with the detector crystal, giving scintillation light photons. The photomultiplier translates the light pulse into an electrical impulse. By means of a series of steps that include defining the photon energy and event placement, the scintillation site and depicts the position of detected events is discovered. (13) The incident photon collisions where incident photons transfer their energy can be located using the position-sensitive detector in the base of the scintillation camera. A sustained scintillation crystalline nature is mapped by many photomultiplier tubes in the classic gamma camera configuration (PMTs).

Manufacturers employ different numbers, shapes, and sizes of PMTs; the end component is not a photodetector that mimics a point or a pencil. A small beam of light photons is produced by the scintillation light, but this beam diverges and spreads throughout the crystal before taking the shape of a cone at the PMT end and lighting several PMTs. (13)

Since one PMT typically gets the most light produced by the scintillation process,

the location of contact might be inferred to rely on a single PMT signal. To be able to spatially detect the amount of radioactivity in a human organ, an electronic circuit in the detecting equipment that can distinguish the region of the generated gamma radiations is essential. The addition of all PMT signals should, in theory, boost location positioning accuracy. (13)

2.2.1 Collimators

Gamma radiation from a radioactive substance is distributed uniformly throughout a sphere. They are not similar to photons, in which it is possible to focus on a particular spot using optical lenses. Gamma radiation generated from a radionuclide that has been injected into a patient can be found by enabling photons that travel in a certain route to interact with the crystal. A multi-hole aperture, also referred to as a collimator, allows us to accumulate and characterize the radioactivity that is dispersed throughout different tissues (13). When using a parallel hole collimator, only photons that are parallel to the detector layer pass through the collimator holes. Meanwhile, the collimator septa effectively absorb entering from any other angle. As a result, only photons moving naturally toward the detector may have any impact on the image that is formed, giving rise to a representation that is closely tied to the radiopharmaceutical's radioactive radiation's spatial variability (14). A lead slab with a sequence of holes and septa positioned in a preset geometric design works as the collimator. The geometric placement of the holes and septa detects the kind and operation of the collimator. Unfortunately, it is not possible to observe most of the gamma radiation released by an administered radioisotope with the gamma camera as so much radiation does not pursue the directions provided by collimator holes (13). The detection of gamma rays by the detector system occurs at a rate of around 1 in 100,000 photons, making it a terribly inefficient technique that yields poor count data (13). Various sorts and designs have been suggested by nuclear medicine institutes and are now being used. Although parallel hole, converging, diverging, and other types of collimators are typically employed in nuclear medicine imaging, pinhole collimators are a unique class that has shown effectiveness in small animal imaging and have a great intrinsic spatial resolution. One or more of the geometric properties that separate one kind from another is the structure, shape, and height of the collimator holes. (13).

- Low-energy all-purpose (LEAP) (or low-energy general- purpose, LEGP) collimator

- Low-energy high-resolution (LEHR) collimator
- Low-energy high-sensitivity (LEHS) collimator
- Medium- and high-energy (ME and HE, respectively) collimators

Leveraging its longer, narrower holes, LEHR collimators offer a low acceptance angle. This enhances the spatial resolution of the obtained images and aids in the resolution of tiny details. Additionally, it keeps resolution at a distance and is advised in cardiac SPECT imaging because the heart's distance from the detector's surface varies.

In comparison to high-resolution (HR) collimators, LEGP collimators have wider acceptance angles and significantly bigger hole diameters. Compared to the LEHR collimator, it has higher sensitivity and lesser spatial resolution qualities. In tests that demand a high count rate (like dynamic studies), LEGP collimators are helpful in increasing sensitivity because the spatial resolution has less of an impact on how the images should be interpreted. The GP collimator significantly outperforms the HR collimator in terms of sensitivity with just a slight reduction in measurement resolution due to differences in the hole's diameter and length, as well as the septal thickness of both collimators. It should be noted that different manufacturers have unique designs and label their products differently. For illustrate, the collimator parameters offered to a GP collimator are possibly totally identical to ones given to the same type of collimator by another producer (15).

When compared to other collimators with the same acquisition time, LEHS collimators have good count rate capabilities and provide images with minimal statistical noise. However, this is accomplished by compromising on the obtained images' resolution characteristics. In other words, the rise in sensitivity came at the expense of the ability to discern minute structures. HE and ME collimators, significant-energy radionuclides like I-131 and Fluorodeoxyglucose-F18 (FDG), and medium-energy radionuclides like gallium-67 and In-111 have high penetrating powers and may therefore penetrate collimator septa, raising background images and potentially impairing spatial contrast. Compared to lower-energy collimators, ME and HE collimators feature thicker septa and offer less transparency to high-energy gamma rays. By destroying small-size lesions, radionuclide experiments using ME and HE collimators show reduced spatial resolution (17). As a result, partial volume averaging results in decreased quantitative precision. But if there are alternative sources with higher-energy gamma rays, ME collimators can be advised above LE collimators in investigations needed low-energy photons (such as

iodine-123) in order to reduce septal penetration artifacts and boost quantitative accuracy (13).

New collimators having a unique plan that can preserve the resolution and sensible points of the examination while offering lesser septal penetration were introduced by several manufacturers as a remedy to the issue. When compared to parallel-hole collimators with the same size exit plane, convergent and divergent collimators have a distinct field of view. The field of view offered by diverging collimators is greater than that offered by parallel-hole collimators, whereas it is lower for convergent collimators. The direction of the holes diverges in diverging collimators when viewed from the collimator's back surface (the face opposing the crystal). They are employed in small-field-of-view cameras to reduce the amount of big organs that are projected onto the camera crystal. From the viewpoint of the collimator's rear surface, converging collimators have holes that are converging (16). Special varieties of gamma camera collimators include cone beam and fan beam. The former features a single focal point for each collimator hole that is situated a specific distance from the collimator surface and is known as the focal point. At the collimator's center, the focal length is the shortest and progressively gets longer as it moves outward. Each row of collimator holes in the fan beam collimator has its own focal point, and all of the focal points combine to form the collimator's focal line. In order to provide independent and nonoverlapping projection profiles, it has parallel collimation with the axial direction of the subject and converging collimation inside each slice. This design enables the use of a streamlined slice-by-slice picture reconstruction method. However, because the holes are axially and transaxial involved in cone beam geometry, image reconstruction is made more difficult. With a relative improvement in count sensitivity, which is greatest at the focal site, a converging collimator gives a magnified picture of small objects discovered at places between the collimator surface and the focal point/line. They are particularly useful for some applications, such as brain tomography. The sensitivity grows progressively from the collimator surface until the source reaches the focal point, whereas the resolution of the converging collimator is at the highest rate at the surface and declines with source distance. As a result, the object at greater distances is observed by more holes, improving sensitivity because of the proportion of holes being able to observe the object at a close distance develops with an increase in object distance. Only one direction, usually the transverse direction, is magnified, and the cone beam collimator also amplifies along the axial direction. Reduced field of view and insufficient data for 3D (three-dimensional)

reconstruction are cons of convergent collimators (17).

Pinhole collimator: The pinhole collimator is a vital component that's widely utilized in nuclear medicine labs, particularly in small-organ imaging like thyroid and parathyroid scans. Additionally, it is helpful for the pediatric population, bone joints, and skeletal extremities. It has a few millimeter-wide apertures and is a cone-shaped structure comprised of lead, tungsten, and platinum (2 6 mm). The aperture size of the small-animal pinhole collimator can be reduced to 1 2 mm or even less to satisfy the resolution demands imposed by tiny structures and minute tracer uptake. 20 to 25 cm is the length of the collimator from the point of the aperture to the back surface. Lens equations can be used to explain image production in the sense that the data collected show an inverted and magnified image. A magnified image of small objects produced by the pinhole collimator gives the appearance of an increase in spatial resolution (18).

2.2.2. Crystal

After passing through the collimator holes, the incident photons come into contact with the scintillation crystal. The crystal must be chosen before being used in the design of a gamma camera based on a few advantageous characteristics. Better imaging performance is made possible by scintillators with high density, high atomic number, quick decay time, high light output, and inexpensive cost. In the field of diagnostic radiology, there is no perfect detector material, but most frequently, the material that is chosen has some desirable qualities that make it preferable over alternatives (13).

Table 2.1. Properties of scintillation crystals used in gamma camera

	Na(Tl)	Csl(Tl)	CsI(Na)
Density (g/cm3)	50	4.51	4.51
Decay time (ns)	230	1000	630
Photon yield (keV)	38	45 52a	39
Refraction index	1.85	1.8	1.84
Hygroscopic	Yes	Slightly	Yes
Peak emission (nm)	415	540	420

The sodium iodide crystal with thallium activation NaI(Tl) is the commonly often applied detector item for gamma cameras. Gamma rays are transformed into light quanta by the scintillation phenomena and then amplified by a PMT to create an observable electrical signal. Scintillation happens as a photon strikes a crystal and interacts with it to create photoelectrons or Compton scattering. The resultant electrons from photoelectric or Compton interactions move quickly in the crystal to create additional interactions between the atoms and molecules of the crystal, such as excitations or ionizations. In order to return to the ground state and deexcite these exciting products, scintillation light is released (13).

2.2.3. Photomultiplier tube (PMT)

An essential piece of hardware in the gamma camera's detection mechanism is the PMT. Its major job is to turn the scintillation photons into an electronic signal that can be detected. As depicted in Fig. 1, the PMT is a vacuum tube was occurred by an anode, a photocathode, focusing electrodes, and electron multipliers (dynodes). The PMT has a long past in a variety of fields, including medicine and other scientific disciplines including high-energy physics and spectrophotometry (19).

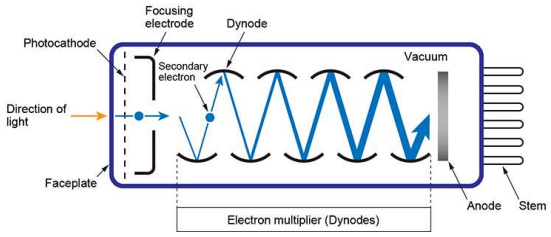

Figure 2.1. View of PMT

2.3. Radiation Interaction with Matter

Both the radiation's type and the makeup of the matter have always had an impact on what happens when radiation interacts with matter. The process will start when radiation energy is transferred to the matter's atoms and molecules, heating it or even changing its structure. If a bombarding particle or photon transfers its whole amount of energy, the radiation will be seen to cease on the inside of the irradiated material. The remaining energy, on the other hand, will appear as if the matter were transparent or at least translucent if the energy is not entirely implanted in the matter. Having said that, we will now discuss some of the processes that arise when radiation interacts with matter. Especially, we will first explore individually how photons (such as gamma and x-rays) and charged particles interact with matter (alpha and beta particles) (20).

2.3.1. Interaction of Photons with Matter

Photons come into contact with atoms as they move through matter. The sort of interaction relies on both the atomic number (Z) and the energy of the photons that constitute the matter. Compton scattering is the predominant type of interaction in materials with lower atomic numbers, such as human tissue (Z = 7.5), when nuclear medicine is practiced using gamma rays with intensities between 50 keV and 550 keV. With respect to interactions, lead (Z = 82) is a case of a material with a higher atomic number where the photoelectric effect predominates. Pair formation, a third sort interaction between photons and matter, only happens at very high photon energy (more than 1020 keV), hence it is unimportant in clinical nuclear medicine. (20).

2.3.2. Compton Scattering

In Compton scattering, an incident photon gives some of its energy to an outer shell electron, or (basically) a "free" electron, which causes the electron to be ejected from the atom. This electron is known as a Compton electron after being ejected. Depending on how much energy is transmitted from the photon to the electron, the photon is dispersed at a specific angle. Nearly 0 to 180 degrees can be found in the scattering angle range. (20). The scattering angles of 135° and 45° are shown in Figure 2.2.

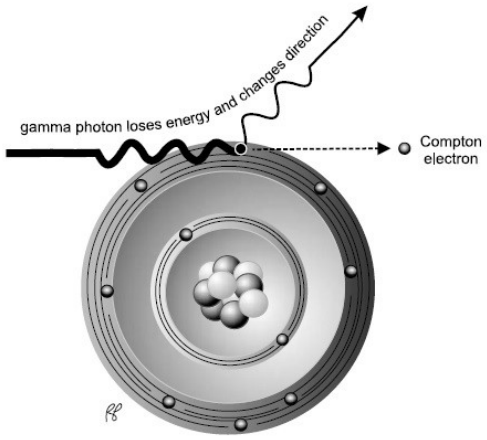

Figure 2.2. Compton Scattering

2.3.3 Photoelectric Effect

A low-energy gamma ray or one losing the majority of the energy due to Compton

interactions might impart its residual energy to an orbital electron which is usually an inner-shell electron. The emitted electron is recalled as a photoelectron, and the mechanism is known as the photoelectric effect. With the energy of the incident gamma ray lessened by the binding energy of the electron, this electron has the same energy when it departs the atom. The inner-shell vacancy is subsequently filled by an outer-shell electron, and the extra energy is released as an x-ray (21).

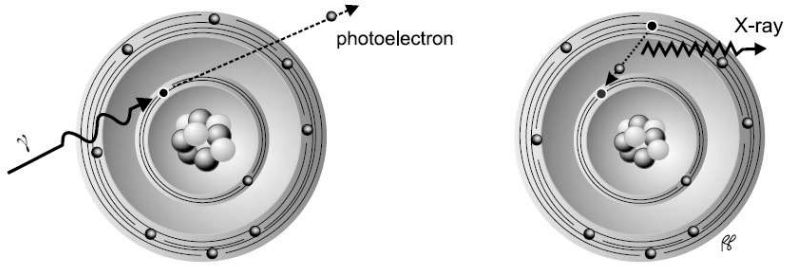

Figure 2.3. Photoelectric Effect

2.3.4. Attenuation of Photons in Matter

The intensity of the beam (stream of photons), that is, the number of photons still in the beam, diminishes when the beam travels through matter due to the interactions between photons and matter. Attenuation describes that loss of photons and the material through which the beam travels is related to the attenuator. Attenuation, in more precise terms, is the ratio of the beam's intensity (I_{out}) to its initial intensity (I_{in}) when it enters the attenuator. The attenuator's thickness, x, measured in centimeters, is an exponential function of attenuation. The fact that the function is exponential can be suggested to indicate that, if half of the beam is lost by passing through the first centimeter of material, the remaining half will also lose half while passing through the following centimeter, and so on. It is similar to the exponential decay of radioactivity over time (20).

$$I_{out} / I_{in} = e^{-(\mu x)}$$

Where the attenuator's property is the linear attenuation coefficient. The linear attenuation coefficient is represented as "per centimeter" when the thickness is specified in centimeters, as is typically the case. As may be predicted, dense tissue, like bone, has a higher linear attenuation coefficient than soft tissue, like fat. In general, the average atomic number (Z) and thickness of the attenuator, as well as the energy of the photons, all affect the linear attenuation coefficient (20).

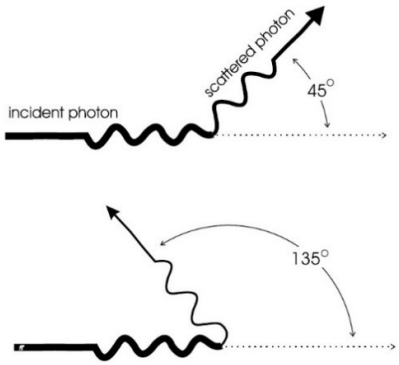

Figure 2.4. Angle of photon scattering

The linear attenuation coefficient is discriminated by the density of the attenuator to create a new term, the mass attenuation coefficient (μ/ρ). The mass attenuation coefficient is measured in units of cm2/gram when a material's density is specified in $^{g}/_{cm^3}$.

Another part of the attenuation process is called radiation absorption. The enpowering of the beam as it moves through matter is referred to as attenuation. The transfer of energy from the beam to the substance is referred to as absorption (20).

2.4. Interaction of Charged Particles with Matter

Charged particles can be easily halted by matter due to the strong electrical force that exists between them and the atoms of an absorber. They move more energy over a closer distance and come to rest faster than photons do. They are referred to as nonpenetrating radiation because of this. An electron with this energy would not penetrate soft tissue more than 0.00014 cm, unlike a photon with 100 keV.

2.4.1 Excitation

The electrons encircling the atom's nucleus interact with charged particles (alphas, betas, and positrons) by giving up some of their kinetic energy. Often, the energy from a low-energy particle is only enough to move an electron from the atom's inner to its outer shell. Excitation is the procedure in question. The process of de-excitation occurs after excitation when the displaced electron swiftly moves back to the lower-energy shell and releases its newly obtained energy as an x-ray. The x-ray is accepted as a characteristic x-ray owing to the fact that there is equality between obtained energy to the difference in

the binding energies of the electron shells, and the binding energies of the electron shells are founded by the atomic formula of the element (20).

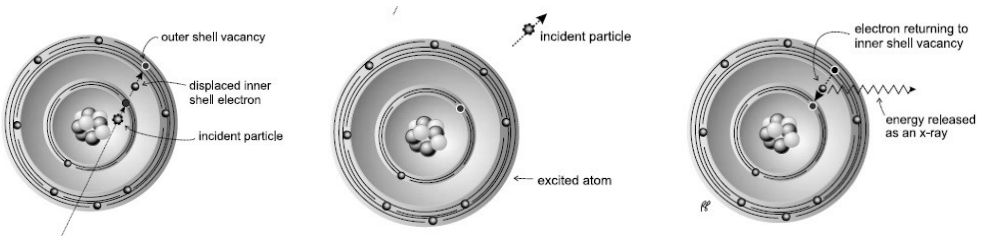

Figure 2.5. Excitation and De-Excitation

2.4.2. Ionization

Charged particles with adequate energy can also provide an electron, usually one in the outer shell, enough energy to evict it from the atom. We refer to this process as ionization. The unbound electron quickly fills this hole in the outer shell. An outer shell electron is expected to "drop" into the inner shell hole when an inner shell electron is ionized (a much less common occurrence), and a distinctive x-ray is to be released. Ionization is not just the result of charged particles interacting with materials.(20).

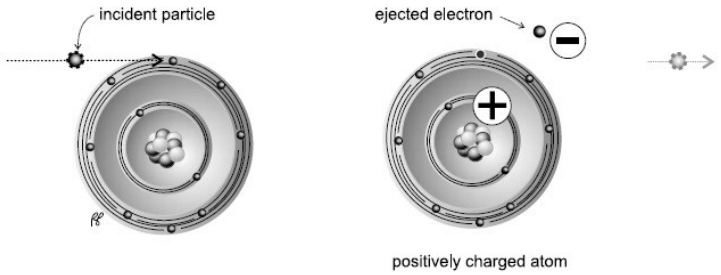

Figure 2.6. Ionization

2.4.3. Specific Ionization

The positively charged and free atom and negatively charged electron occur when radiation forces an electron out of an absorber's atom is known as an ion pair. The materials in the absorber are characterized by the energy transferred per ion pair produced, W. For each ion pair produced in air or water, for instance, roughly 33 eV (within the range of 25 eV to 40 eV) is transmitted to the absorber. The term "specific ionization" is frequently used to refer to the number of ion pairs produced for every unit

of radiation travel (SI).(20).

2.4.4. Linear Energy Transfer (LET)

The amount of energy transferred over a specific distance by a particle passing through an absorber is known as linear energy transfer (LET). Specific ionization is connected to linear energy transfer.

$$LET = SI \times W$$

Beta particles and photons are categorized as low LET radiation, while alpha particles are considered high LET radiation (20).

2.4.5. Range

The range is the length of time radiation stays inside the absorber. When compared to heavier, more charged (such as alpha particles), less energetic particles, which are lighter, less charged, and/or have greater energy, move further. Every time an electron interacts with an absorber's atoms while crossing one, energy is lost. Variable energy is lost during each encounter. As a result, there is a 3%–4% range in the overall distance moved by electrons of the same energy. The straggling of the ranges is the name given to this range variation. The heavier alpha particles show very little range of straggling and are not significantly impacted (20).

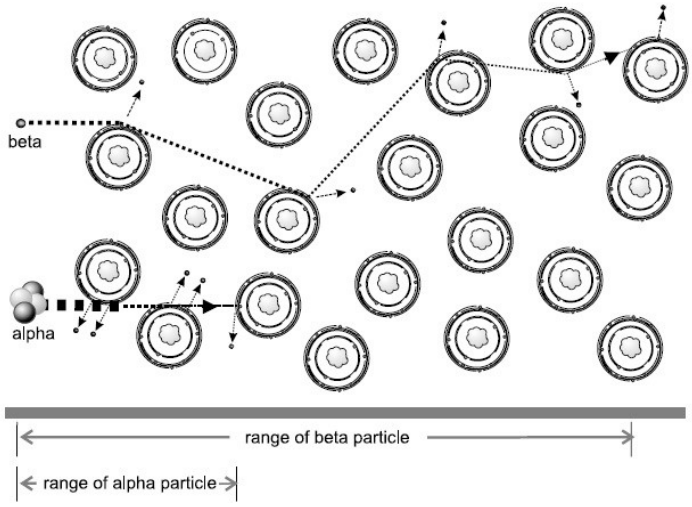

Figure 2.7. Particle Range

2.4.6. Annihilation

The most frequent kind of this interaction in the matter is between an electron and a positron (positive electron) (negatron). A positron merges with a free or loosely bound negative electron after having most of its kinetic energy transferred through ionization and excitation. Remember that positrons and electrons have the opposite electric charge despite having the same mass. This reaction is explosive because the total mass of the two particles is quickly transformed into two photons with opposing directions and energies of 511 keV each. A destruction reaction is what is happening in this case. Another illustration of how mass and energy can be interchanged is provided by the following: E = mc2, or energy, is defined as mass times the square of the light speed (21).

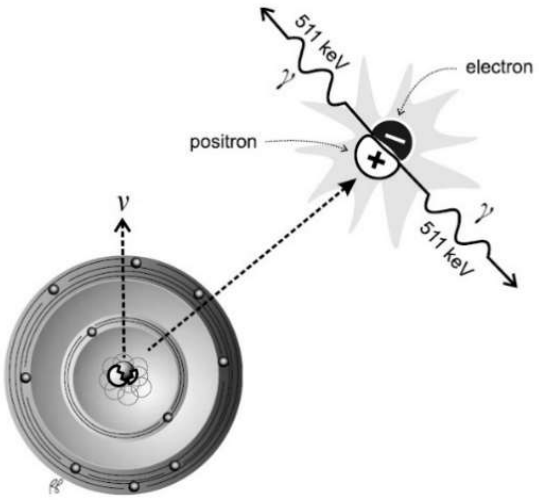

Figure 2.8. Annihilation Reaction

2.5. Monte Carlo Simulations and GATE

A mathematical method called Monte Carlo Simulation, widely related to the Monte Carlo Method or a multiple probability simulation, is utilized to guess the likely results of an unknown event. As to facilitate judgment in ambiguous situations, John von Neumann and Stanislaw Ulam developed the Monte Carlo Method during World War II. Since the estimation method is based deeply on chance, much like a game of roulette, it was called Monaco because of a well-known casino town.

Monte Carlo Simulations are being used to assess the effects of risk in a variety of real-world contexts, involving stock markets, artificial intelligence, sales forecasting, managing projects and cost. Moreover, they suggest a lot of pros on predictive models

with stable inputs, along with the capability to run sensitivity analyses and figure out the association of inputs. Decision-makers can apply sensitivity analysis to understand how various inputs affect a specific outcome, and they can try correlation to detect the relations among any input variables. (22)

- A Monte Carlo simulation is a type utilized to guess the possibility of a variety of results when the potential for random variables exists.
- Monte Carlo simulations aid in expressing the effect of risks and being unclear in guess on and forecasting models.
- A Monte Carlo simulation demands nominating multiple values to an unclear variable to succeed in multiple results and then averaging the results to gain an idea.
- Monte Carlo simulations propose perfectly efficient markets. (23)

When we compare it with a set of fixed input values, Monte Carlo Simulation assumes a set of results relying on a foreseen range of values. Namely, for any variable that has inherent uncertainty, a Monte Carlo Simulation designs a model of possible choices by internalizing a possibility distribution, like a uniform or normal distribution. Afterward, applying a new set of random values among the minimum and maximum values, frequently calculates the results. That method can be done tens of thousands of times in a typical Monte Carlo experiment to get a variety of possible solutions.

In addition, Monte Carlo Simulations are possible to be utilized because of their precision in long-term presumes. You can observe project results much more precisely further into the future as the number of forecasts expands as well as the number of inputs. When a Monte Carlo simulation ends, it produces a list of possible results along with the likelihood that each one will happen.

Calculating the chance of rolling two regular dice is a basic example of a Monte Carlo simulation. There are 36 different methods to roll the dice. Based on this, you can manually calculate the possibility of a particular result. To get a more correct prediction, you can model rolling the dice 10,000 (or more) times applying a Monte Carlo simulation. (22)

2.6. GATE Simulation Platform

GATE combines unique characteristics related to emission tomography with the pros of the GEANT4 simulation toolbox, involving well-validated physics models, detailed geometry descriptions, and sophisticated modeling and 3D rendering tools. There are several hundred C++ classes in it. The GEANT4 kernel is supported by a core layer of C++ classes that control time, geometry, and radioactive sources. A user class deriving from the core layer classes may be implemented in an application layer, allowing the creation of certain geometrical volume forms and/or the specification of operations on these volumes, also including rotations and translations. The use of GATE does not necessitate C++ programming as the application layer has so far implemented all necessary features. Rather, a dedicated scripting mechanism widely recognized as the macro language, which extends GEANT4's native code interpreter, is used to perform and manage Monte Carlo simulations of realistic setups. (23)

GATE's capacity to align all time-dependent components to enable a clear explanation of the acquisition process is one of its most novel properties. Following the geometry definition, scripting can be used to make the geometry's components move. The evolution of the source activity is preserved in sync with all of the geometrical elements' movements. The acquisition is divided into a number of time steps for this purpose, during which the geometry's constituent parts are viewed as being at rest. As to the decay kinetics of each radiopharmaceutical, decay intervals are constructed inside these time steps; in this way, the number of events declines exponentially from time step to time step and also within each time-step. This supports the event-by-event modeling of time-dependent phenomena like count rates, chance coincidences, or detector dead time. Further, it is possible to generate realistic detector output using the interaction histories from GEANT4. In GATE, the user can create a linear processing chain to replicate a detector's electronic response, including its energy resolution, trigger performance, and cross-talk. (23).

3. MATERIALS AND METHODS

3.1. Gamma Camera System

To perform NEMA measurements with phantoms, GE Discovery 670 SPECTCT system installed in Yeditepe University Kosuyolu Hospital is used (Figure 3.1).

Figure 3.1. GE Discovery 670 SPECTCT system

The published specifications of the Gamma Camera are given in Table 3.1. similarly, specifications of the collimators used in the thesis are indicated in Table 3.2.

Table 3.1. Gamma Camera Specifications of D670 SPECTCT System

Crystal Material	Crystal Thickness	Number of PMTs	UFOV (cm)	Energy Range	Intrinsic Energy Resolution(FWHM)	Intrinsic Uniformity at UFOV(Differential)
NaI(Tl)	3/8 inches	59	54x40	40-620 KeV	9.5%	≤ 2.3%

PMT: Photo multiplier tube
UFOV: Useful field of view
NaI(Tl): Sodium Iodide

Table 3.2. Collimator Specifications of LEHR and LEHRS Collimators

Collimator Name	FOV(cm)	Hole Type	Hole Diameter(mm)	Septal Thickness (mm)	Hole Length (mm)
LEHRS	54x40	Hex	1.43	0.13	32
LEHR	54x40	Hex	1.5	0.2	35

3.2. Image Quality Parameters Measurements with Gamma Camera

Following tests performed with Gamma Camera as explained in NEMA Standards Publication "NU-1:2012 Performance Measurements of Gamma Cameras" (24).

- Intrinsic spatial resolution
- Intrinsic count rate performance in air (copper plates method)
- System planar sensitivity and collimator penetration and scatter
- System spatial resolution without scatter
- System spatial resolution with scatter
- SPECT reconstructed spatial resolution without scatter
- SPECT reconstructed spatial resolution with scatter
- System volume sensitivity

Tests types with collimators named started with "System" and run for LEHR ve LEHRS. (24).

3.2.1. Intrinsic Spatial Resolution

The smallest object that can be resolved on the image in terms of size is referred to as spatial resolution. The smallest resolvable item in a digital image cannot be smaller than the pixel size, which sets a resolution limit. The instantaneous field of view of the sensor, being a measurement of the ground area observed by a single detector element in a particular instant in time, plays a major role in determining an imaging system's intrinsic resolution. Other variables that cause the image to blur frequently diminish this resolution.

According to NEMA NU-1:2012 standard (24). Test setup for Intrinsic Spatial Resolution states that Tc-99m is the radionuclide used in this test. A source holder that protects the source from objects like walls, ceilings, and people while letting the source's gamma flux to access the camera. Tc-99m energy window suggested by manufacturer used. The maximum count rate did not overpass 20000 cps during the test (24).

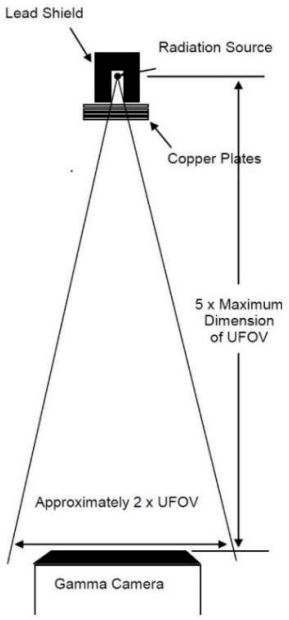

Figure 3.2. Intrinsic Spatial Resolution Test Setup

The test phantom is a lead mask with parallel slots that are 1 mm wide. The test phantom placed as close as practical to the crystal that covers the entire UFOV. The geometry for a rectangular field of view [FOV] requires adjacent slit centers to be 30 mm apart from one another. For Tc-99m, the mask's thickness is 3 mm.

The camera detector placed with one of the parallel slits on the lead mask vertical to the measurement axis. The radionuclide is a single point source that is centered with respect to the detector UFOV and at least five times farther away than the UFOV's maximum linear dimension above the lead mask with parallel slits.

It is advised to use a digital resolution that is 0.2 times the estimated FWHM. The digital resolution should be 30 mm in a direction parallel to the slits. In order to create line spread functions with a width of 30 mm or less, the data from a two-dimensional matrix must be added accordingly to the direction of the slits. Each cumulative line spread function's peak channel must include at least 10,000 counts.

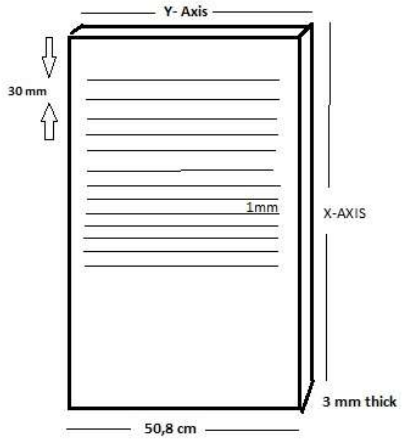

Figure 3.3. NEMA Intrinsic Spatial Resolution Phantom

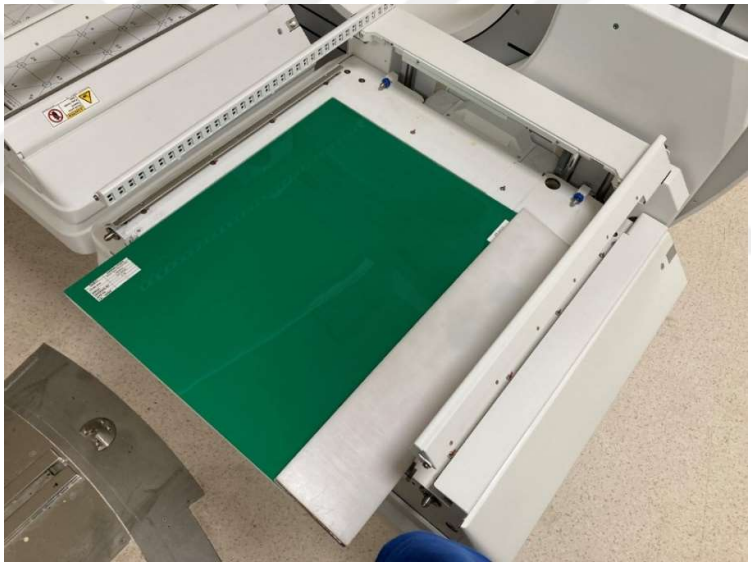

Figure 3.4. Intrinsic spatial resolution phantom setup

- High concentration of ^{99m}Tc (10 mCi) in 0.5-0.8 ml located over the center of detector about 5 FOV away.
- Static acquisition with 1024x1024 matrix, 1.0 zoom set and 15000 kcounts collected.

After the imaging, line profiles created on the slits and the graphs fitted with Gaussian function. FWHM values coming from the fitted graph calculated both for UFOV and CFOV. For these calculations Origin Pro8 software used (24).

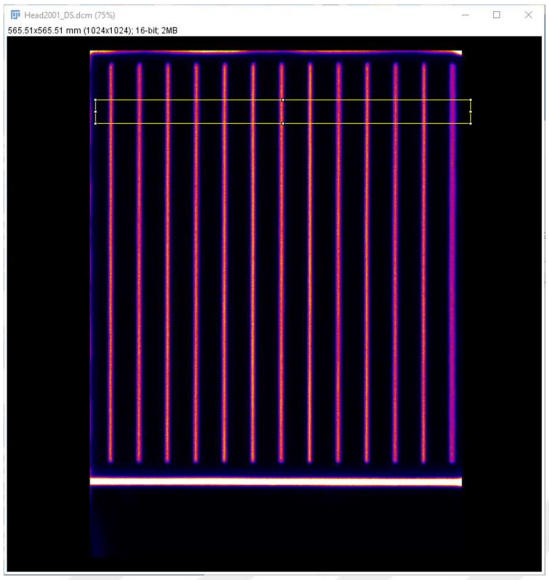

Figure 3.5. Intrinsic resolution and linearity feature of ImageJ software

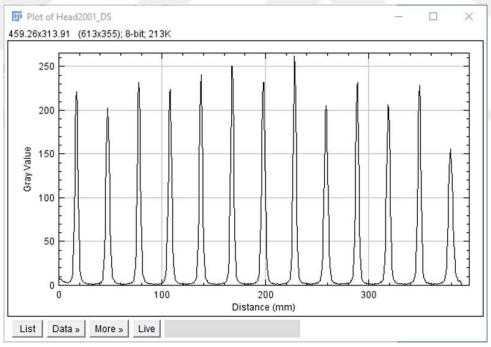

Figure 3.6. FWHM and FWTM calculation page of Origin Pro8 software

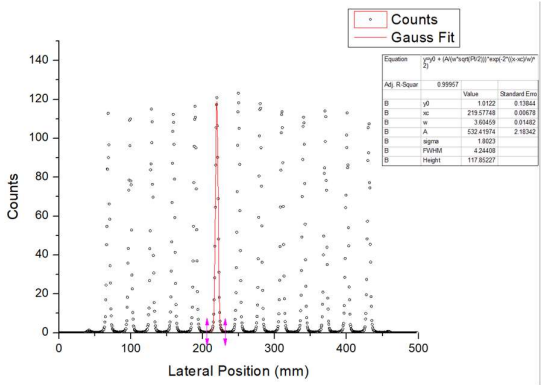

Figure 3.7. Fitting FWHM with Gaussian function in Origin Pro8 software

3.2.2. Intrinsic Count Rate (Copper Plates Method)

The performance of the count rate can be examined using the copper plates method. The measured count rate with a 20% count loss and the maximum count rate both need to be assessed and reported. Measurements of both parameters must be done without artificial scatter. It is required to provide the observed vs input count rate curve. It is ideal to assess gamma camera count rate performance as part of acceptance testing and some accreditation agencies also demand that it be done annually.

Test Setup for Intrinsic Count Rate (Copper Plates Method); Tc-99m is the radionuclide used in the test. 15mCi of Tc99m activity prepared. Collimators uninstalled from gamma camera and scanner positioned with L-Shape in order detector to face to radioactive source. Before the test, scanner room background measurement done with 256x256 matrix, 1.0 zoom during 100 seconds. The manufacturer's suggestion for the proper diagnostic mode followed when determining the energy window for Tc-99m. Peaking done at a low count rate and did not manually change while the test is executing. The camera performed the test in the proper clinical mode.

Figure 3.8. Intrinsic count rate copper plate method test setup

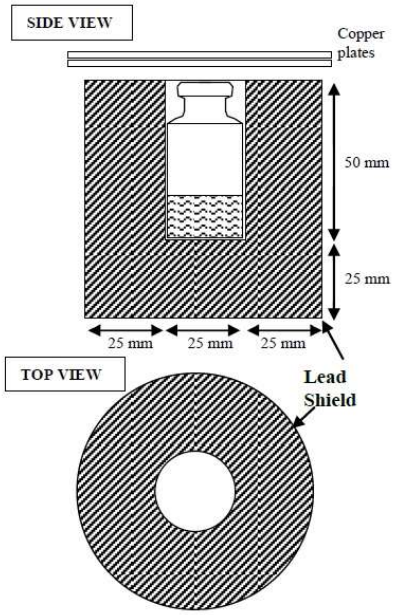

Figure 3.9. Intrinsic Count Rate Test Source and Copper plates Setup

15 Copper plates with 2.5mm thick have used during the test. After background test following acquisitions repeated by reducing one copper plate on each scan.

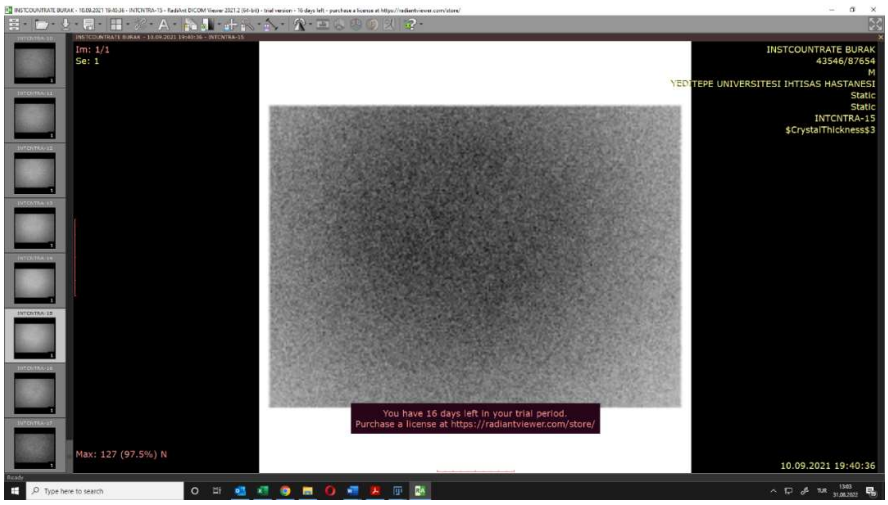

Figure 3.10. Intrinsic Count Rate Test Images

Following calculations and analysis have completed after the scans:

- Each data point is initially background-corrected with following formula:

$$C_i = K_i - R_{bkg} \cdot \Delta t_i \quad (3.1)$$

Where:

C_i: Backround corrected total count

K_i: Total count

R_{bkg}: Backround count rate

Δt_i : Scan time in seconds

- Each data point's observed count rate (OCRi) calculated using the following formula:

$$OCR_i = \frac{C_i \ln(2)}{T_{half} \cdot [1 - exp\left\{(-\Delta t_i) \cdot \frac{\ln(2)}{T_{hal}}\right\}]} \quad (3.2)$$

Where:

T_{half} : 21.672 seconds; half life of Tc-99m

Δt_i: Scan time in seconds

- Fitting the data at low count rates produces the input count rate (ICRi). The OCRi is corrected for source decay between measurements before fitting the data. Decay Corrected OCR (OCRi,DC) is calculated as follows:

$$OCR_{i,DC} = OCR_i \cdot exp\left(\frac{(t_i - t_n) \cdot ln}{T_{half}}\right) \quad (3.3)$$

Where:

t_i: The start time of acquisition

t_n: The end time of acquisition

- All OCRi values below 20,000 cps (or fewer, depending on the detector's count rate characteristics) must have a natural logarithm that can be fitted to a straight line:

$$ln(OCR_{i,DC}) = a.(N_n - N_i) + b \quad (3.4)$$

- The following formula is then used to determine the input count rate (ICRi).

$$ICR_i = \exp(a.(N_n - N_i) + b) \,.\, exp\left\{\frac{(t_n - t_i).ln2}{T_{half}}\right\} \quad (3.5)$$

Where:

N_n: total number of copper plates that produce OCRi of less than 20000 cps

N_i: number of copper plates

The plot of OCRi vs ICRi is than created (Figure 3.11). on the graph the maximum OCRi value is reported besides the count rate at 20% loss is also reported. The value is determined from graph by intersection of count rate curve and OCR=0.8 × ICR, as shown in the Figure 3.10. (24).

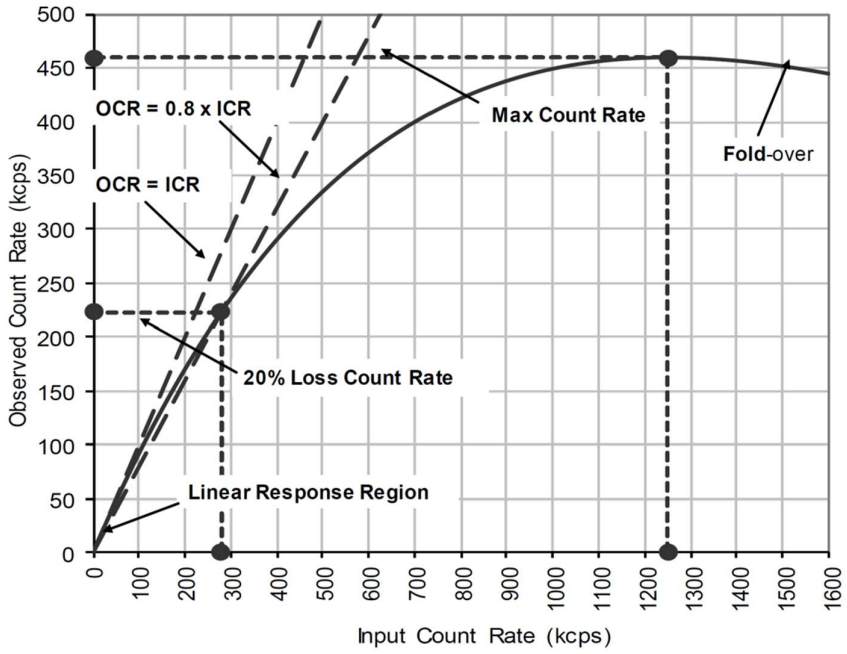

Figure 3.11. Intrinsic count rate plot

3.2.3. System Planar Sensitivity and Collimator Penetration and Scatter

The ratio of collimated counts measured in one acquisition plane to the activity of a certain planar source located accordingly to that plane is called system planar sensitivity. However, counts that are detected can also result from radiation that penetrates through the collimator's septa or scattered off the septa and is picked up. The overall image quality is degraded by both penetrating and scattered radiation, which should be taken into account separately from the sensitivity resulting from accurately collimated counts. The collimator properties, source, and system parameters all impact the penetration and scatter as well as the system's planar sensitivity. Therefore, unless specifically stated differently, the design of these system variables used for this assessment should be the same as that used in an appropriate clinical mode.

For each type of collimator (LEHR and LEHRS) the system's planar sensitivity and collimator penetration fraction determined using the Tc99m and the results reported in cps/MBq and percent, respectively.

Test setup;

Well maintained dose calibrator, a 150 mm-diameter flat plastic, a 1-5 cc syringe, a 30-50 cc syringe, and other test supplies are needed for this measurement

Using the large plastic syringe, the flat plastic dish filled with water until the bottom is completely covered, about 2-3 mm deep. Using a dose calibrator, the source activity (A_{SR}) inside the small plastic syringe must be properly quantified. The final step in the phantom preparation is to spread this source from this syringe into the flat dish.

To determine the quantity of activity in the phantom at the time of preparation, $A_{Cal} = A_{SR} - A_{Res}$, the residual activity still remaining in the syringe, A_{Res}, measured in the dose calibrator.

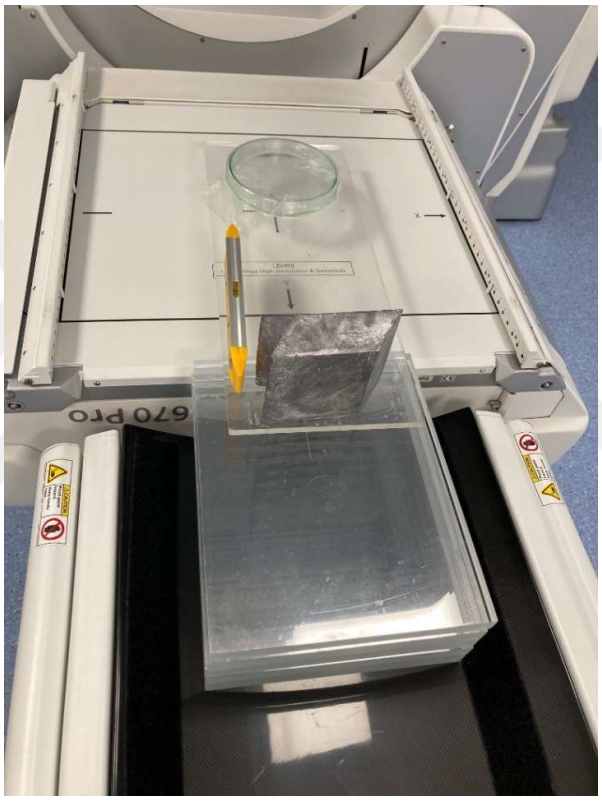

Figure 3.12. System planar sensitivity test setup

The prepared phantom positioned so that its bottom inner face is 10 mm from the detector's face, and positioned close to the FOV's center. There was no dispersion material in the area. In order for the activity to be distributed evenly, the phantom's base was on level.

Utilized the imaging system to gather four million counts. All uniformity corrections disabled for counts which is recommended. The acquisition's start time recorded with the stated level of precision.

This measurement repeated using the phantom's bottom inner face for the same number of counts (20mm, 50mm, 100mm, 150mm, 200mm, and 250mm) from the face of collimator.

Following analysis and calculations done after the acquisitions;

The counts in a circular region of interest (ROI) summed that is centered over the area of activity and is 60% the phantom's diameter for each acquisition. Included the centers of all pixels in the ROI (24).

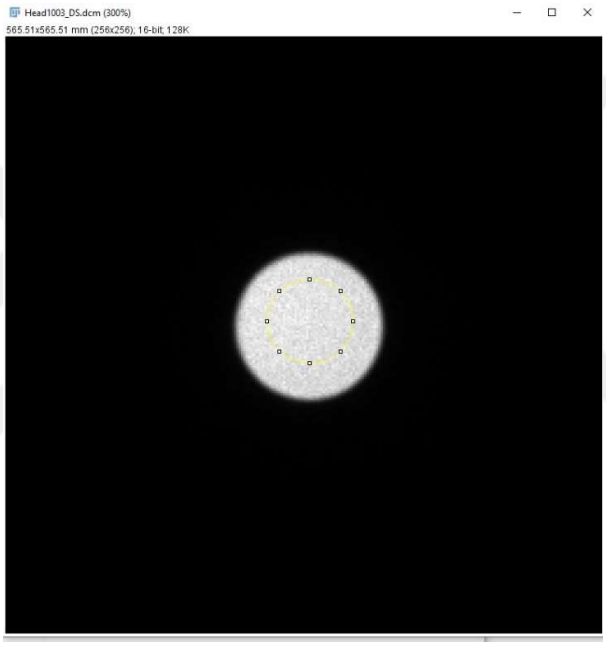

Figure 3.13. Circular ROI that is centered over the area of activity and is 60% the phantom's diameter.

- Decay corrected count rate calculated with the following formula:

$$R_i = C_i \exp\left(\frac{(T_i - T_{cal})}{T_{half}} ln2\right) . \left(\frac{ln2}{T_{half}}\right) . (1 - \exp\left(-\frac{T_{acq,i}}{T_{hal}} ln2\right))^{-1} \quad (3.6)$$

Where:

R_i: Decay-corrected count rate

C_i: Summed counts over the circular ROI

T_i: start time of the acquisition

$T_{acq,i}$: Duration of the acquisition

T_{cal}: Time of activity calibration

T_{half}: Half life of Tc99m (21672 seconds)

The decay-corrected count rates and the distance between the detector and the phantom fitted to the function using the typical Levenberg-Marquardt non-linear least squares fit method:

$$R_i = c_0 + c_1 \exp(-c_2 D_i) \quad (3.7)$$

Where:

c_0, c_1 and c_2 are the parameters in fitting function and D_i is the detector face to bottom of the phantom distance. The penetration fraction (PF) calculated with the following formula where $D_N = 100mm$.

$$PF = \frac{c_1 \exp(-c_2 D_N)}{c_0 + c_1 \exp(-c_2 D_N)} \quad (3.8)$$

Sensitivity calculation is possible when summing whole image acquired from 100mm distance. Decay corrected total count rate measured with the following formula:

$$R_{D=100} = C_{D=100} . \exp\left(\frac{(T_{100} - T_{cal})}{T_{half}} ln2\right) . \left(\frac{ln2}{T_{hal}}\right) . (1 - \exp\left(-\frac{T_{acq.100}}{T_{half}} ln2\right))^{-1} \quad (3.9)$$

Where:

$R_{D=100}$: Decay corrected count rate at 100 mm

$C_{D=1}$: Summed counts at 100 mm over the whole image

System sensitivity (S_{TOT}) calculated for each collimator set (LEHR and LEHRS) with the following formula:

$$S_{TOT} = \frac{R_{D=100}}{A_{cal}} \quad (3.10)$$

3.2.4. System Spatial Resolution without Scatter

The mentioned test with both LEHR and LEHRS collimator pairs assessed and reported as FWHM and FWTM of the line spread function. How well an imaging system's individual parts cooperate to produce the final image is indicated by its extrinsic performance.

Test Setup for System spatial resolution without scatter; Tc-99m is the radionuclide for the test. Count rate did not surpass 20000 cps. For the energy window, manufacturer's recommended settings was used.

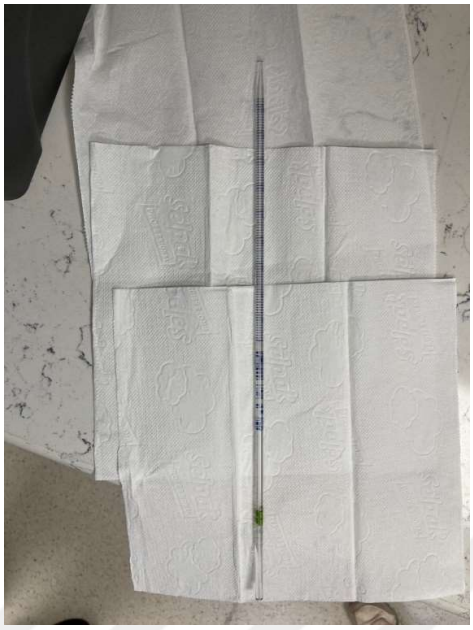

Figure 3.14. One of capillary tube for system spatial resolution test

Two capillary tubes the inside diameter is less than 1mm was used for the test. The active lenght of tubes was 240 mm. 10 mCi of Tc-99m filled inside the capillary tubes with 1cc plastic syringe.

The other capillary tube also positioned 100 mm from the face of the collimator and 100 mm away from, and parallel to, the first capillary tube.

To collect 15000 kcount, 512x512 matrix size, 1.0 zoom was set for the static acquisition settings.

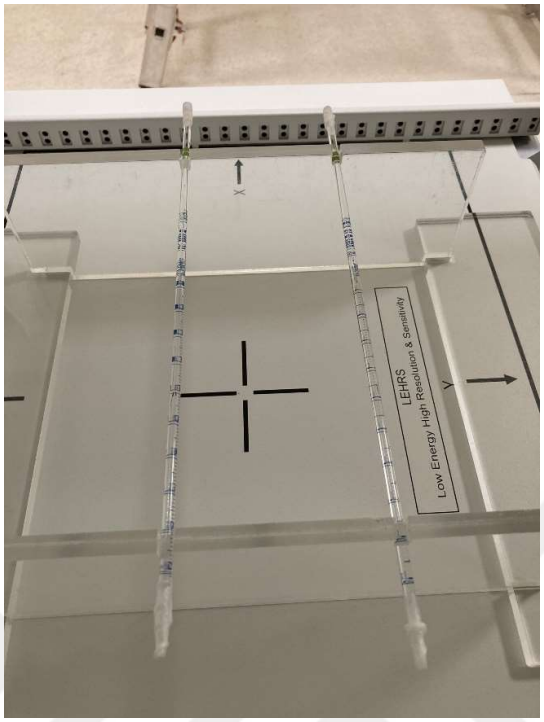

Figure 3.15. Two capillary tubes positioning parallel to collimator surface

After the acquisition FWHM and FWTM measurements values converted from pixel to millimeter per pixel values with using System Spatial Resotion and Pixel Size feature under NMQC tab of ImageJ software (24).

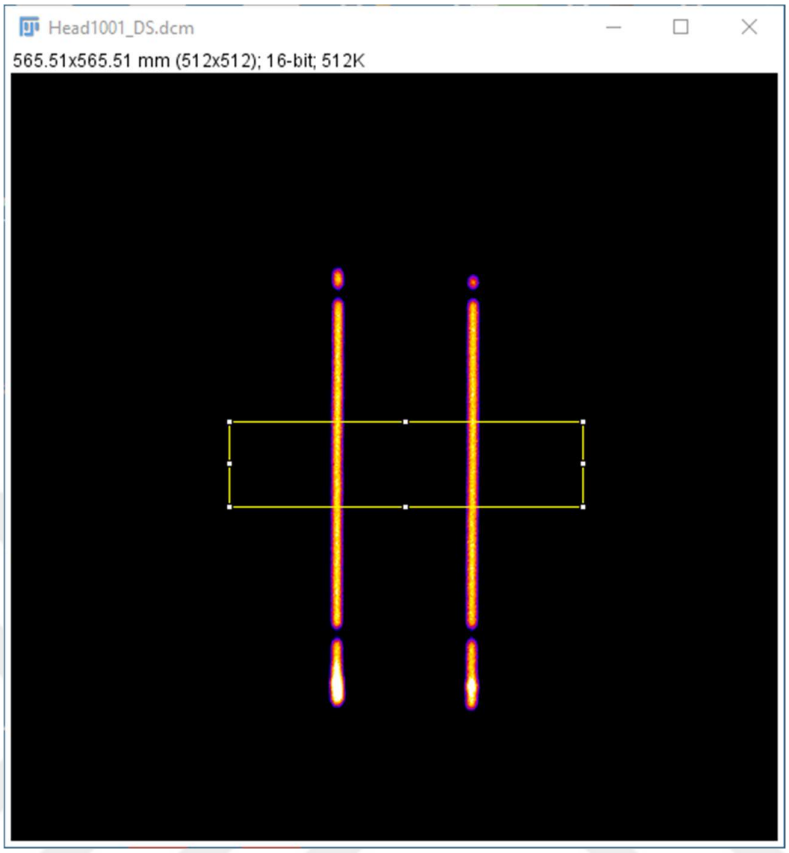

Figure 3.16. System spatial resolution calculation of ImageJ software

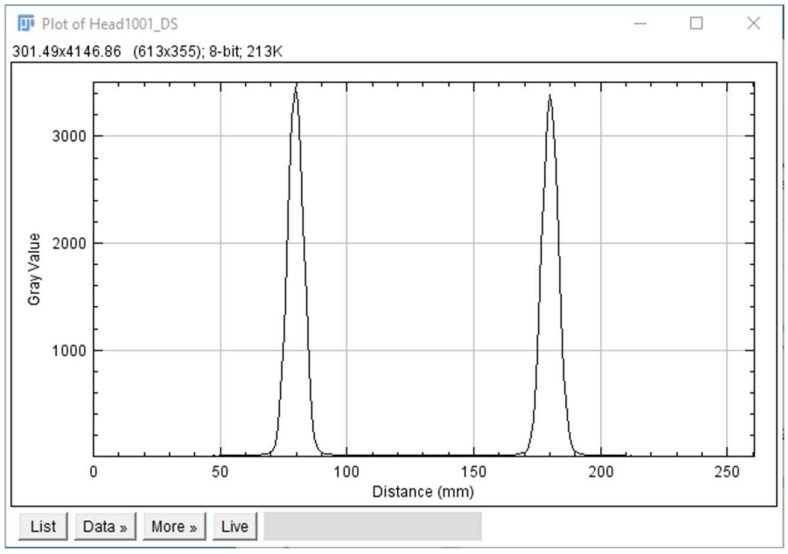

Figure 3.17. FWHM and FWTH calculation of test Origin Pro8 software.

3.2.5. System Spatial Resolution with Scatter

The mentioned test has been assessed and explained as FWHM and FWTM. The expectation was to meet manufacturer's specs on the measured values. Since two types of collimators which are LEHR and LEHRS used for measurements, measurement results reported for both collimator types.

The radionuclides employed for the test was Tc-99m. During the measurements for both LEHR and LEHRS collimators, count rate did not exceed 20000 cps.

Two capillary tubes the inside diameter is less than 1mm was used for the test. The active lenght of tubes was 240 mm. 10 mCi of Tc-99m filled inside the capillary tubes with 1cc plastic syringe. 5 PMMA blocks positioned, 100 mm total between capillary tubes and detector surface. Also 2 PMMA blocks have put on top of plastic holder which is 50mm.

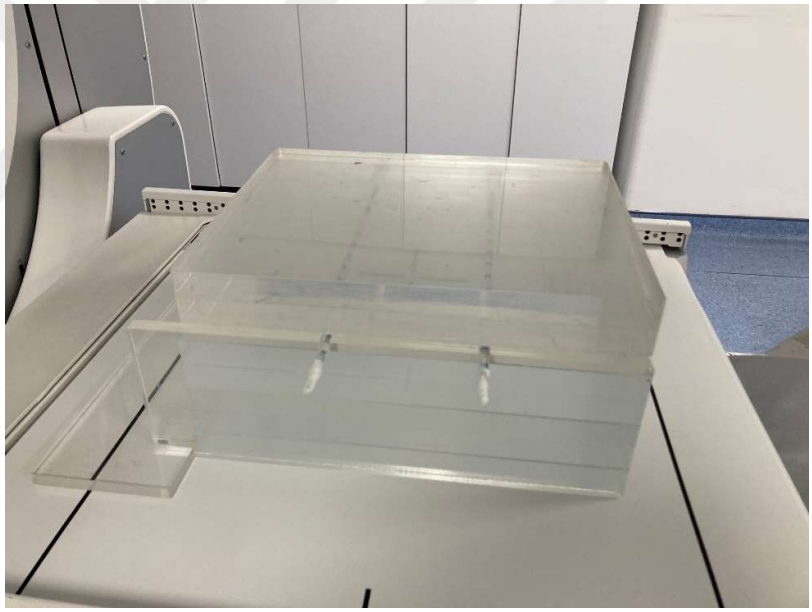

Figure 3.18. System spatial resolution with scatter measurement phantom setup

Same measurements done with the System spatial resolution without scatter. The only difference is to have scatter material during 100 mm between source and detector and the the scatter material during 50 mm behind the source.

The Tc-99m injected into the capillary tubes. One of the capillary tubes must be placed as near to the opposite side of the 100 mm-thick acrylic scattering block, which is placed directly in front of the collimator. The second 50 mm thick scattering block placed on the other side of the capillary tube.

Static acquisition with 512 × 512 matrix, 1.0 zoom setup to collect 10000 counts.

FWHM and FWTM values converted from pixels to milimeters using milimeters per pixel calibration with using Orijin software (24).

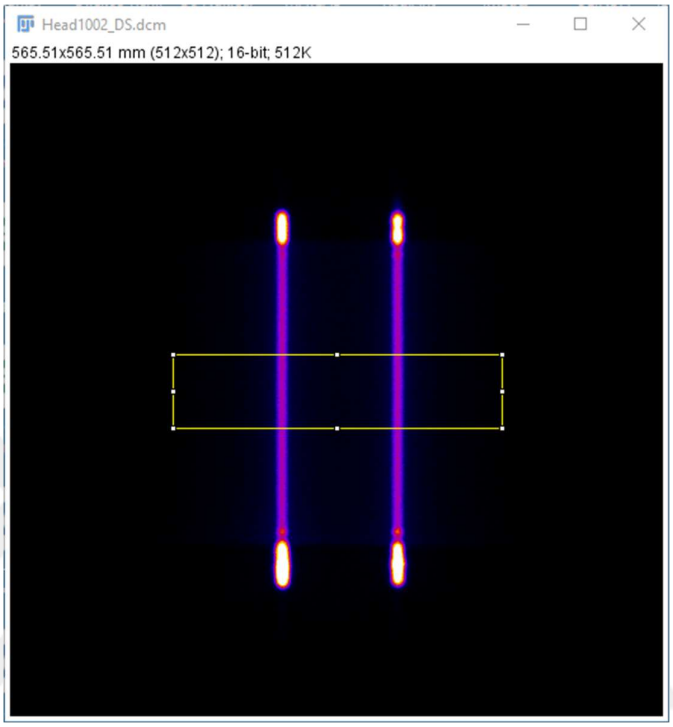

Figure 3.19. System spatial resolution view of ImageJ software

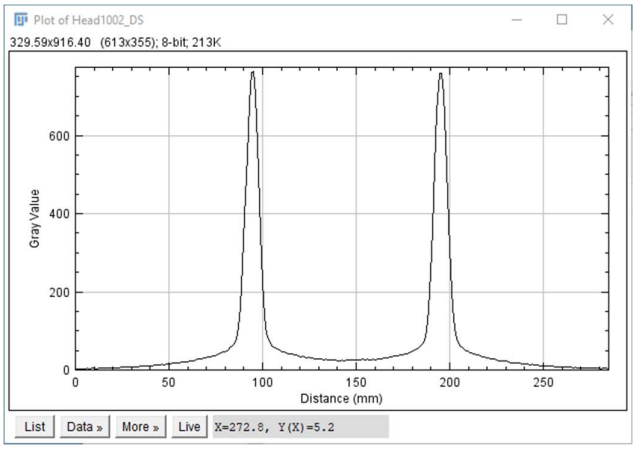

Figure 3.20. Calculation of FWHM value with Orijin software

3.2.6. SPECT Reconstructed Spatial Resolution without Scatter

The mentioned test assessed at three specific source in air. FWHM values of resolution in X, Y and Z directions calculated and reported. Three Tc-99m sources used for the measurement. Count rate did not exceed 20000 kcount during the acquisition.

Three point sources in capillary tubes positioned as defined in Figure 3.21. There are 50 mm distances between edge points of sources. Also sources positioned parallel to each other with 75mm distances.

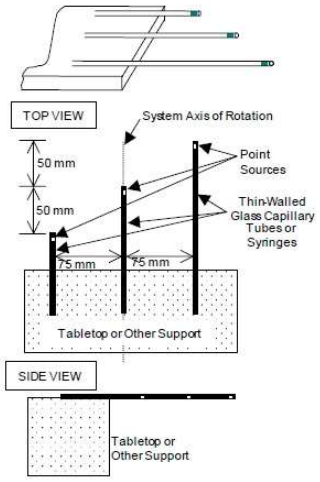

Figure 3.21. Spect reconstructed spatial resolution without scatter test setup

Sources positioned in the center of FOV of detector. The level of three point sources holder parallel to table top. The source in the center positioned to axis of rotation and centered to FOV of detector within ± 5mm. The rotation diameter set 300 ± 10 mm. Total 20000 kcounts collected with 3 degree per step, 128×128 matrix 1.0 zoom factor.

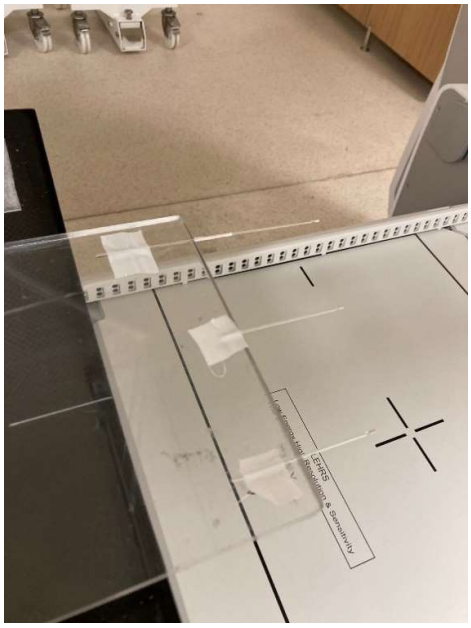

Figure 3.22. Spect reconstructed spatial resolution without scatter source positioning

The raw data reconstructed with Filtered Back Projection (FBP) recon method with Ramp filter with using GE Xeleris 3.1 software.

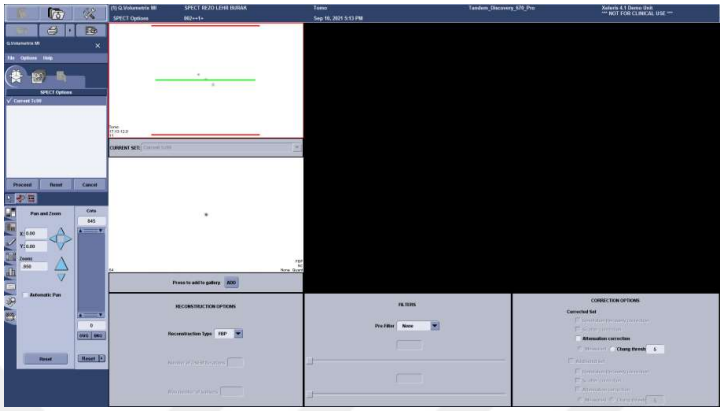

Figure 3.23. FBP reconstruction of raw projection

After the reconstruction, three dataset created from the software which are transaxial, sagital and coronal.

Three point sources contained three summed views (axial, sagital and coronal) became nine point source images after the reconstruction. The images analyzed separately with a ROI centered on the maximum count pixel related with this point.

Each point consolidated in the figure – Y position to define the image X - position point spread function. Also consolidated in the image – X position to define the image – Y direction.

FWHM and FWTM calculated from the data points can be observed as sample in Figure 3.24

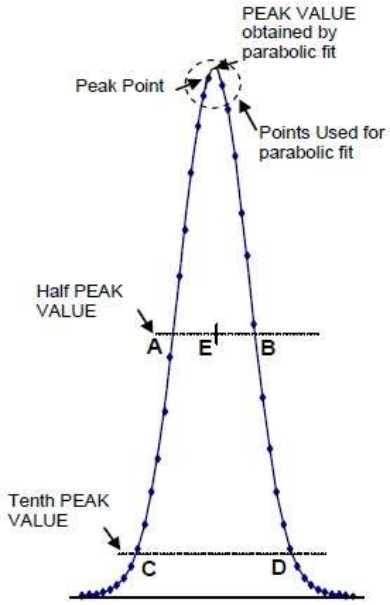

Figure 3.24. Plot over the data points of the measurements

B – A = FWHM in channels

D – C = FWTM in channels

$\frac{A+B}{2}$= E: peak center

Based on standard NEMA document following calculations done with the respected formulas:

$$Central\ Transaxial\ \equiv \frac{(X_{c,t}+X_{c,c}+X_{c,t}+X_{c,s})}{4} \quad (3.11)$$

$$Central\ Axial\ \equiv\ \frac{(Z_{c,s}+Z_{c,c})}{2} \quad (3.12)$$

$$Peripheral\ Radial \equiv (\frac{X_{pl,t}+X_{pl,c}+X_{pr,t}+X_{pr,c}}{4}) \quad (3.13)$$

$$Peripheral\ Tangential\ \equiv (\frac{Y_{pl,t}+Y_{pl,s}+Y_{pr,t}+Y_{pr,s}}{4}) \quad (3.14)$$

$$Peripheral\ Axial\ \equiv (\frac{Z_{pl,s}+Z_{pl,c}+Z_{pr,s}+Z_{pr,c}}{4}) \quad (3.15)$$

After the calculations:

- Central Transaxial (X,Y)
- Central Axial (Z)
- Peripheral Radial (X)
- Peripheral Tangential (Y)
- Peripheral Axial (Z)

Values reported. For the above calculations, ImageJ software used.

First a ROI created as shown in Figure 3.25

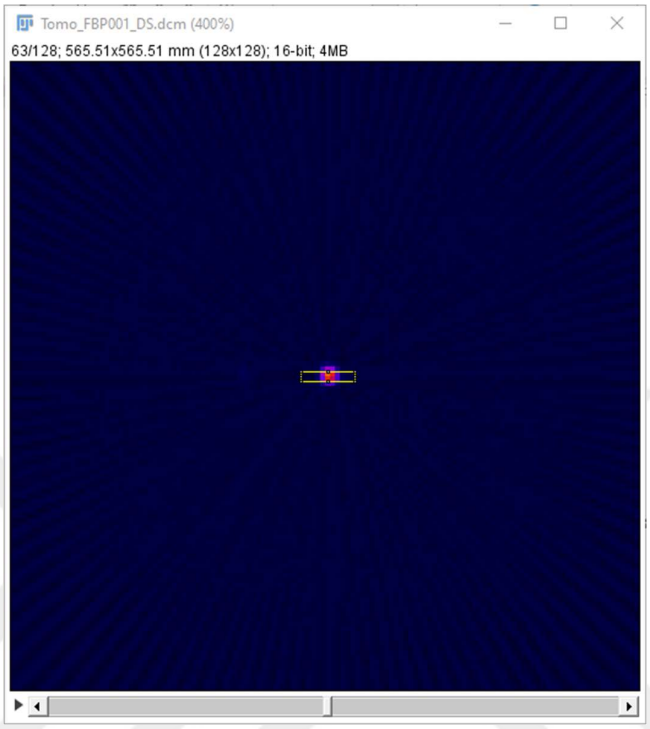

Figure 3.25. ROI creation in ImageJ software

Second step is to creation the plot values based on the ROI as shown in Figure 3.26

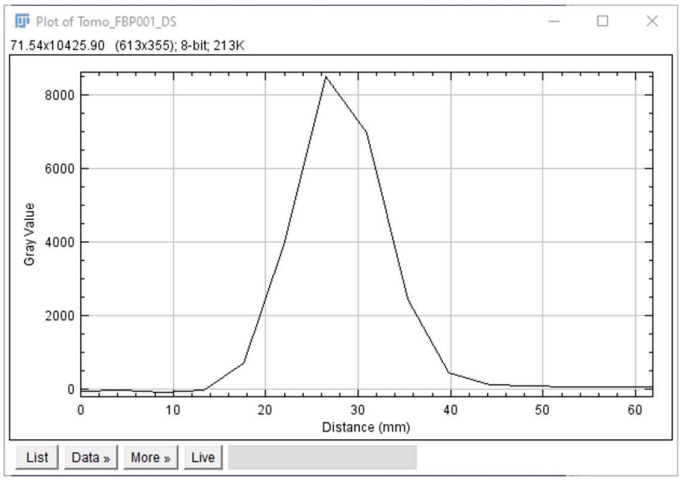

Figure 3.26. Creating plot values with ImageJ software

Third step is to select and copy the data points over the plot as shown in Figure 3.27

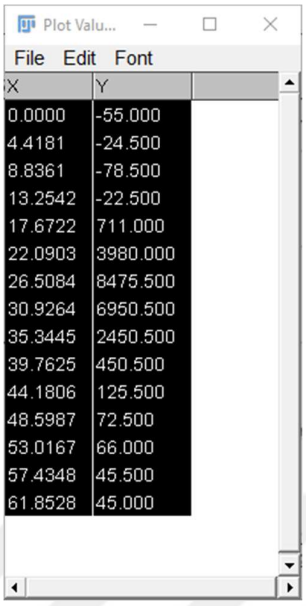

Figure 3.27. Selecting data points from ImageJ

Fourth step is to fit the data points over a Gaussian function in ImageJ software with using curve fitting feature as shown in Figure 3.28

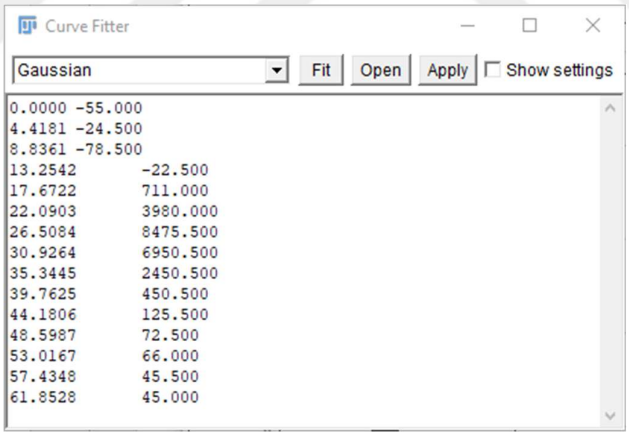

Figure 3.28. Curve fitting in ImageJ software

As last step data points (a,b,c,d) collected to calculate FWHM values as shown in Figure 3.29

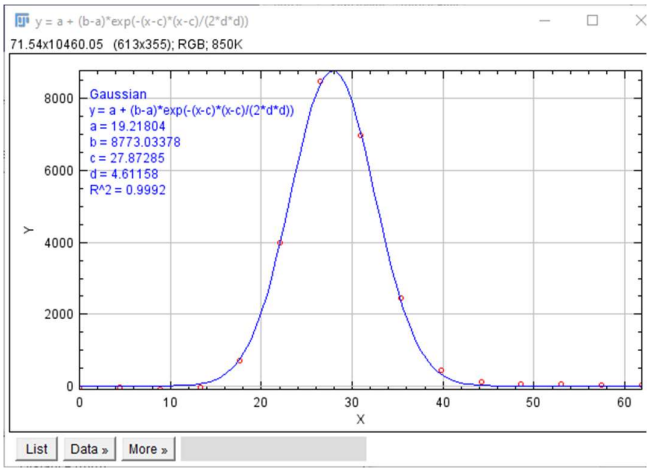

Figure 3.29. Collecting data points after fitting the curve

The mentioned calculations and measurements have completed for both LEHR and LEHRS collimator pairs (24).

3.2.7. SPECT Reconstructed Spatial Resolution with Scatter

The mentioned test calculated from needed reconstructed transaxial series with triple line sources in a water filled cylinder.

Used radioactive material was Tc-99m, count rate did not exceed 20000 cps.

Figure 3.30. Radioactive line sources to insert water filled cylinder

The phantom contains water inside. The inner radius is 100mm and including three axial line sources with 1mm diameter as shown Figure 3.31.

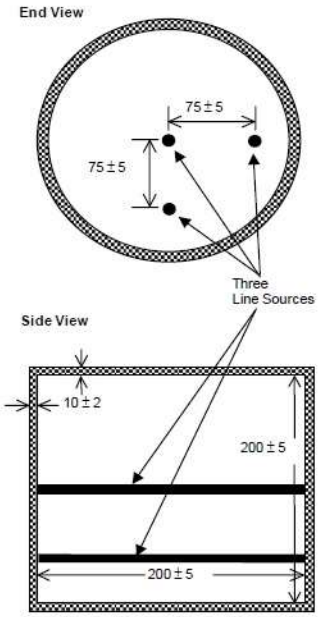

Figure 3.31. Three line source with cylinder phantom diagram

Phantom positioned with the rotation center (COR) and centered in the FOV. Phantom scanned over 360° with circular scan setup. 3° angular step with 128×128 matrix and 20 seconds per step were scanning parameters as shown in Figure 3.32

Figure 3.32. Cylinder phantom setup for system SPECT reconstructed spatial resolution test

After the acquisition raw data reconstructed with Filtered Back Projection (FBP) and Ramp filter. One transverse slice 10±3 mm thickness created. Two more transverse planes each 10±3 mm thickness also were reoccured as shown in Figure 3.33.

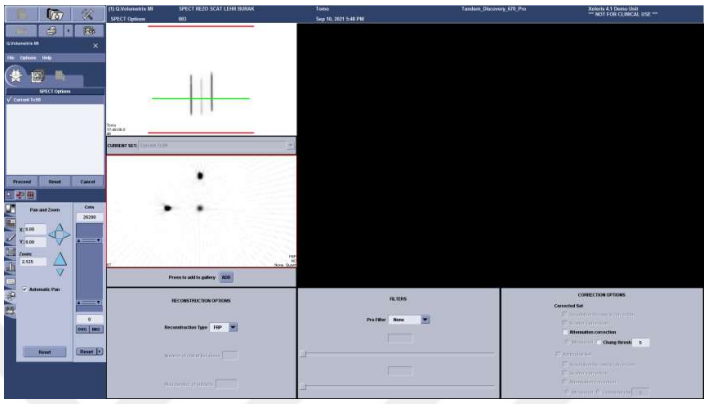

Figure 3.33. FBP reconstruction of acquired data

These three reconstructed points in each of the transverse slices analyzed with ROI where maximum count pixel. FWHM in X and Y determined.

As first step ROI created as shown in Figure 3.34.

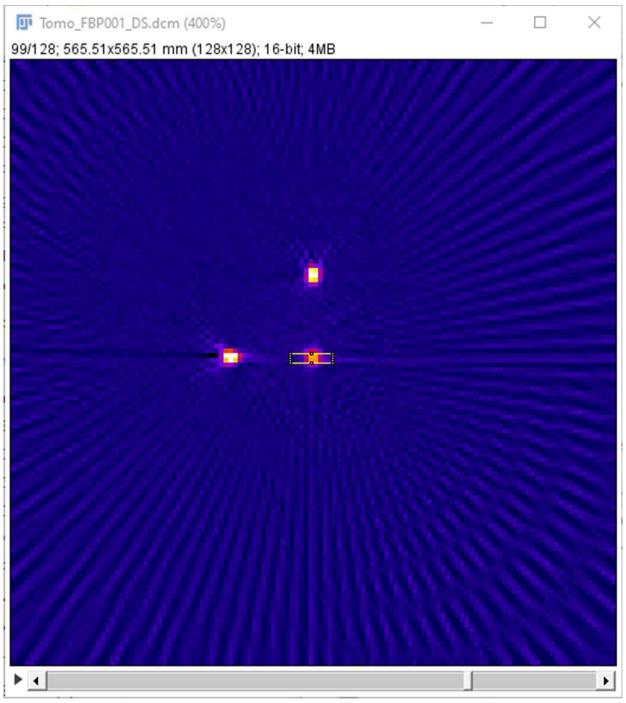

Figure 3.34. ROI creation for calculations

Second step is to creation the plot values based on the ROI as shown in Figure 3.35.

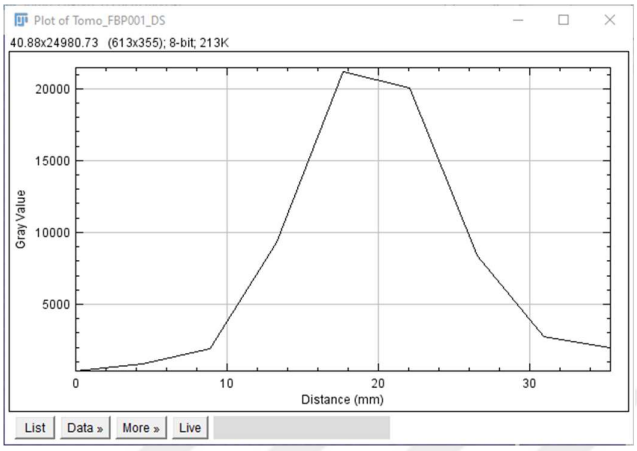

Figure 3.35. Creating plot values with ImageJ software

Third step is to select and copy the data points over the plot as shown in Figure 3.36.

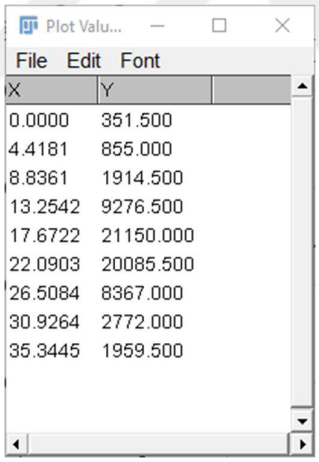

Figure 3.36. Selecting data points from ImageJ

Fourth step is to fit the data points over a Gaussian function in ImageJ software with using curve fitting feature as shown in Figure 3.37

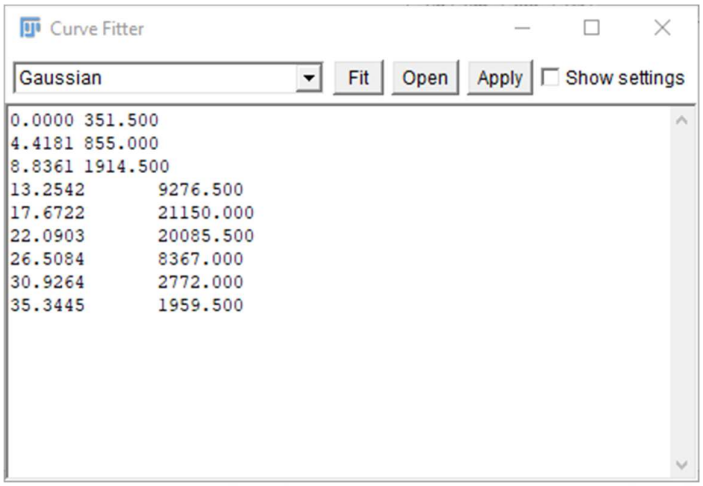

Figure 3.37. Curve fitting in ImageJ software

As last step data points (a,b,c,d) collected to calculate FWHM values as shown in Figure 3.38.

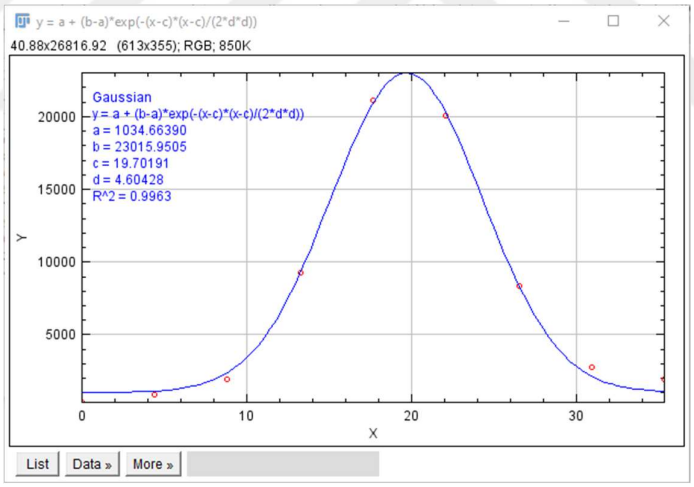

Figure 3.38. Collecting data points after fitting the curve

The mentioned calculations and measurements have completed for both LEHR and LEHRS collimator pairs (24).

3.2.8. System Volume Sensitivity

The test was assessed and approximate volume sensitivity per axial centimeter (VSAC) was declared from this assessment. The SVS measures the responsiveness of the entire system to an even concentration of activity in a particular setup. The axial extent of the cylindrical phantom is used by the VSAC to normalize the SVS. A good estimate

of the overall system reaction to a wide dispersion of activity is provided by the VSAC multiplied by the axial FOV of the system. SVS and VSAC measurements are based on source configuration, radionuclide type, collimator type, detector setup, energy window setting, and other variables.

100 mm – radius cylindrical phantom, syringe, dose calibrator are the test equipment. Known radionuclide activity filled uniformly to cylinder phantom as shown in Figure 3.39

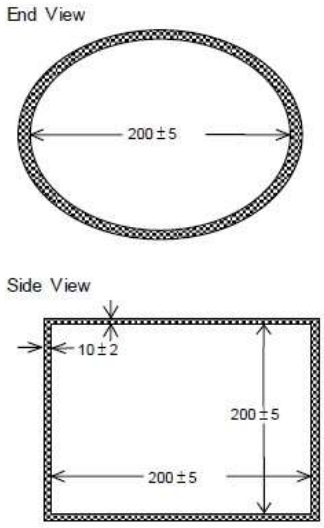

Figure 3.39. System volume sensitivity phantom view

Activity concentration in kBq/cm^3 within specified phantom measured at initial time which is T_i. This calculation gained by discriminated assessed activity in phantom at T_i by volume of phantom.

360° circular SPECT acquisition set with setting 150 mm distance between collimator and phantom. 120 projections collected with 10 seconds of projection time as shown Figure 3.40

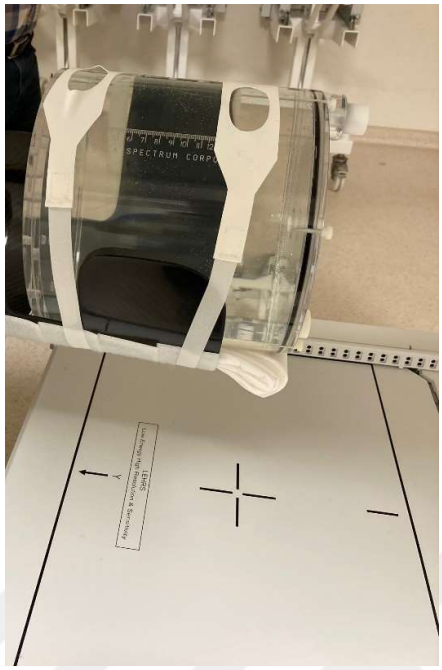

Figure 3.40. SPECT volume sensitivity phantom setup

SVS calculated with following formula:

$$SVS = \frac{A(^{cts}/_{sec})}{B_c(^{MBq}/_{cm^3})} \quad (3.16)$$

VSAC defined by dividing the SVS by the axial lenght or the cylinder.

$$VSAC = \frac{SVS}{Lenght} \quad (3.17)$$

The measurements completed for both LEHR and LEHRS collimators.

3.2.9. Intrinsic Energy Resolution Test

The needed test performed according to instructions of service manual of D670 SPECTCT scanner. Below steps applied for the test:

- Collimators removed and decoy collimators installed.
- Detectors positioned with L-shape to face Tc-99m point source
- 0.5 mCi Tc-99m point source prepared in 0.5 ml of volume inside a plastic syringe
- Before to start energy resolution test, a background measurement performed to verify background activity is less than accepted value according to test prerequisite available in service manual
- After verification of background activity, point source positioned 2 meters away from Detector 1 surface

- Energy resolution test started with using the instruction of user interface of gamma camera
- 1500 kcounts collected for test with 256×256 matrix and 1.0 zoom factor
- Same steps completed for Detector 2.
- Results reported according to NEMA intrinsic energy resolution test reporting instructions (24).

3.3. Gate Monte Carlo Simulation of the Gamma Camera System

For gamma camera simulation with Gate, an input file has *.mac should created works on Linux system. A world defined where gamma camera simulation is going to work in Gate platform.

```
/gate/space/geometry/setXLength 600 cm
/gate/space/geometry/setYLength 600 cm
/gate/space/geometry/setZLength 600 cm
```

After definition of the space where gamma camera is going to be simulated, a box defined which is a known geometry, filled with air.

```
/gate/space/daughters/name Gamma_Camera
/gate/space/daughters/insert box
/gate/Gamma_Camera/geometry/setXLength  10. cm
/gate/Gamma_Camera/geometry/setYLength  40.2 cm
/gate/Gamma_Camera/geometry/setZLength  54.2 cm
/gate/Gamma_Camera/placement/setTranslation  0. 0. 0. cm
/gate/Gamma_Camera/setMaterial Air
/gate/Gamma_Camera/vis/forceWireframe
```

An aluminum box defined to position aluminum frame contains SPECT head which has crystal inside.

```
/gate/Gamma_Camera/daughters/name Al_frame
/gate/Gamma_Camera/daughters/insert box
/gate/Al_frame/geometry/setXLength 4.0 cm
/gate/Al_frame/geometry/setYLength  40.2 cm
/gate/Al_frame/geometry/setZLength  54.2 cm
/gate/Al_frame/placement/setTranslation  2.0 0. 0. cm
/gate/Al_frame/setMaterial Aluminium
/gate/Al_frame/vis/forceSolid
/gate/Al_frame/vis/setColor red
```

3/8' (0.95 cm) NaI crystal with 54×40 cm added inside of aluminum frame. Crystal positioned to left 1mm of aluminum in front of crystal.

```
/gate/Al_frame/daughters/name nai_crys
/gate/Al_frame/daughters/insert box
/gate/nai_crys/geometry/setXLength 0.95 cm
```

```
/gate/nai_crys/geometry/setYLength  40. cm
/gate/nai_crys/geometry/setZLength  54. cm
/gate/nai_crys/placement/setTranslation  -1.425 0. 0. cm
/gate/nai_crys/setMaterial NaI
/gate/nai_crys/vis/forceSolid
/gate/nai_crys/vis/setColor yellow
```

After those settings, 2.5mm thick back compartment added to include glass maden light guide and photo multiplier tubes (PMT). Lateral view of detector is given in Figure 3.41. White box defines the SPECT head, red box defined aluminum frame, yellow box is the crystal and blue box is the back compartment.

```
/gate/Al_frame/daughters/name light_guide
/gate/Al_frame/daughters/insert box
/gate/light_guide/geometry/setXLength 2.5 cm
/gate/light_guide/geometry/setYLength 40. cm
/gate/light_guide/geometry/setZLength 54. cm
/gate/light_guide/placement/setTranslation   0.3 0. 0. cm
/gate/light_guide/setMaterial Glass
/gate/light_guide/vis/forceSolid
/gate/light_guide/vis/setColor blue
```

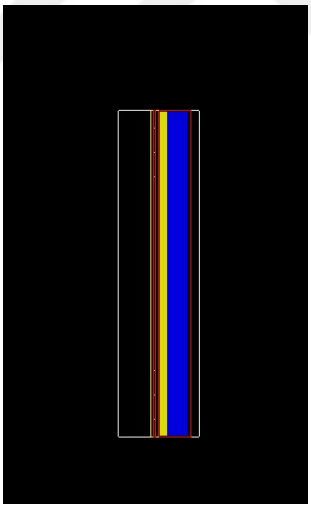

Figure 3.41. Lateral view of detector in Gate.

By those commands, SPECT head for the intrinsic simulations has defined. Starting from aluminum frame through – x coordinate collimator defined. A lead block defined for GE Discovery 670 system LEHR collimator.

```
/gate/Gamma_Camera/daughters/name coll
/gate/Gamma_Camera/daughters/insert box
/gate/coll/geometry/setXLength 3.5 cm
/gate/coll/geometry/setYLength 40.2 cm
/gate/coll/geometry/setZLength 54.2 cm
/gate/coll/placement/setTranslation  -1.75 0. 0. cm
```

```
/gate/coll/setMaterial Lead
/gate/coll/vis/setColor black
/gate/coll/vis/forceSolid
```

A hexagonal hole added to this lead block. Hole geometry is reflecting the specifications of specified collimator. The dimensions of the collimator taken from manufacturer's document.

```
/gate/coll/daughters/name air_hole
/gate/coll/daughters/insert hexagone
/gate/air_hole/geometry/setHeight 3.5 cm
/gate/air_hole/geometry/setRadius 0.075 cm
/gate/air_hole/placement/setRotationAxis 0 1 0
/gate/air_hole/placement/setRotationAngle 90 deg
/gate/air_hole/setMaterial Air
/gate/air_hole/vis/setColor white
/gate/air_hole/vis/forceSolid
```

A rectangular array created by using a repeat vector. Septa thickness – an info coming from manufacturer's specification considered while defining repeat vector (Figure 3.41).

```
/gate/air_hole/repeaters/insert cubicArray
/gate/air_hole/cubicArray/setRepeatNumberX 1
/gate/air_hole/cubicArray/setRepeatNumberY 236
/gate/air_hole/cubicArray/setRepeatNumberZ 184
/gate/air_hole/cubicArray/setRepeatVector 0. 0.17  0.294 cm
```

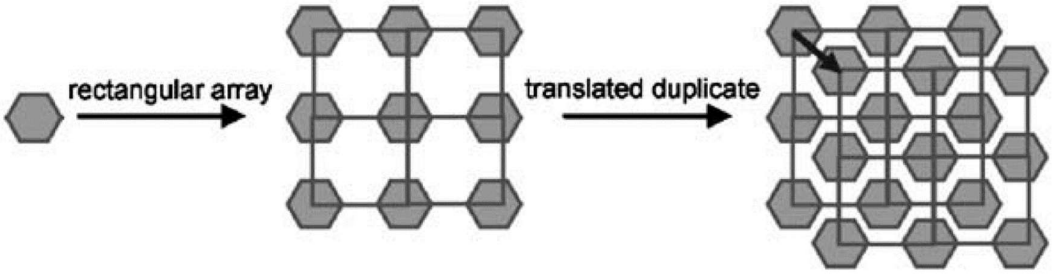

Figure 3.42. Construction of collimator hole

After the creation of array, this array duplicted with a new vector (Figure 3.42).

```
/gate/air_hole/repeaters/insert linear
/gate/air_hole/linear/setRepeatNumber 2
/gate/air_hole/linear/setRepeatVector 0. 0.085 0.147 cm
```

The similar steps were followed for LEHRS collimator with using its specifications. A zoomed view of simulated collimators can be observed in Figure 3.43.

a) 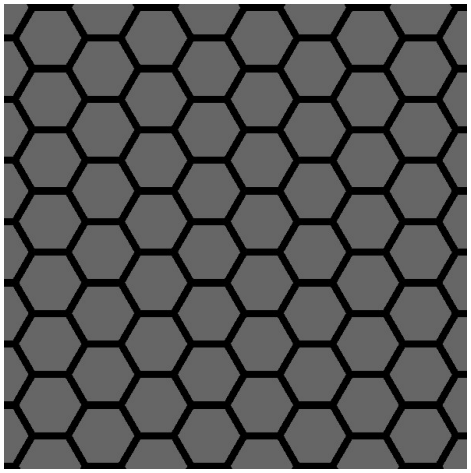 b) 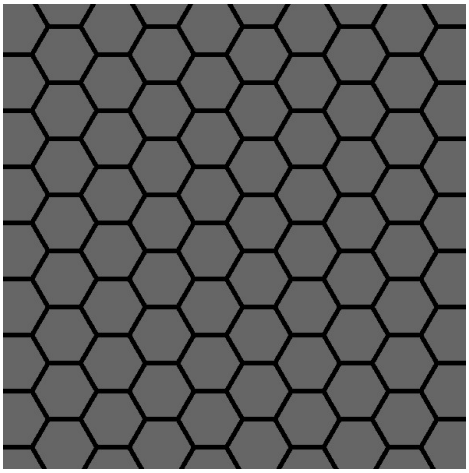

Figure 3.43. a) LEHR and b) LEHRS collimator simulation in Gate

The default physical models for emission tomography are used for all simulations. Following variance reduction technics are used for all simulations.

```
/gate/physics/Gamma/SetCutInRegion      Gamma_Camera 0.1 cm
/gate/physics/Electron/SetCutInRegion   Gamma_Camera 1.0 cm
```

Hereof, the radiation transport terminated when average runaround is below 1mm for gamma lights, 1cm for electrons in SPECT head.

Below defined digitizer features used for SPECT modelling in every simulations.

```
/gate/digitizer/Singles/insert adder
/gate/digitizer/Singles/insert blurring
/gate/digitizer/Singles/blurring/setResolution 3.35
/gate/digitizer/Singles/blurring/setEnergyOfReference 140. keV
/gate/digitizer/Singles/insert spblurring
/gate/digitizer/Singles/spblurring/setSpresolution 9.5 mm
/gate/digitizer/Singles/spblurring/verbose 0
/gate/digitizer/Singles/insert thresholder
/gate/digitizer/Singles/thresholder/setThreshold 126. keV
/gate/digitizer/Singles/insert upholder
/gate/digitizer/Singles/upholder/setUphold 154. keV
```

The energy resolution for 140 keV photons of Tc-99m is to be determined by the method defined in section 3.2.9. The determined value will be added to code assigned by X.XX. The spatial blurring is to be determined from intrinsic resolution simulations by the method defined in section 3.3.1. The determined value will be added to code assigned by Y.YY.

An energy window used in simulations for all gamma camera imaging. This energy window includes 126 KeV threshold and 154 KeV uphold for 140 Kev ±10%. By this means the photons have the mentioned energy been part of imaging.

The output format is selected as ASCII format in every simulation (25).

3.3.1. Intrinsic Spatial Resolution Measurement Simulation

The spatial blurring parameter has to be determined before any simulation. To determine the spatial blurring parameter for the gamma camera simulation, spatial blurring of 2.0, 2.5, 3.0, 3.5 and 4.0 mm defined in intrinsic spatial resolution simulation. For each blurring parameter intrinsic spatial resolution is measured from simulations with the simulated NEMA phantom. To make the simulation, 3mm thick lead plaque added into 1cm thick PMMA phantom. 1mm slits added on to the lead plaque. These slits repeated 13 times in every 3cm (Figure 3.44.a).

```
/gate/Gamma_Camera/daughters/name PMMA
/gate/Gamma_Camera/daughters/insert box
/gate/PMMA/geometry/setXLength 1. cm
/gate/PMMA/geometry/setYLength 40.2 cm
/gate/PMMA/geometry/setZLength 54.2 cm
/gate/PMMA/placement/setTranslation  -.5 0. 0. cm
/gate/PMMA/setMaterial Plexiglass
/gate/PMMA/vis/setColor yellow
/gate/PMMA/vis/forceWireframe

/gate/PMMA/daughters/name nema
/gate/PMMA/daughters/insert box
/gate/nema/geometry/setXLength 0.3 cm
/gate/nema/geometry/setYLength 40.2 cm
/gate/nema/geometry/setZLength 54.2 cm
/gate/nema/placement/setTranslation  0. 0. 0. cm
/gate/nema/setMaterial Lead
/gate/nema/vis/setColor red
/gate/nema/vis/forceSolid

/gate/nema/daughters/name slit
/gate/nema/daughters/insert box
/gate/slit/geometry/setXLength 0.3 cm
/gate/slit/geometry/setYLength .1 cm
/gate/slit/geometry/setZLength 50. cm
/gate/slit/placement/setTranslation  0. 0. 0. cm
/gate/slit/setMaterial Air
/gate/slit/vis/setColor white
/gate/slit/vis/forceWireframe

/gate/slit/repeaters/insert linear
/gate/slit/linear/setRepeatNumber 13
/gate/slit/linear/setRepeatVector 0. 3. 0. cm
```

a) 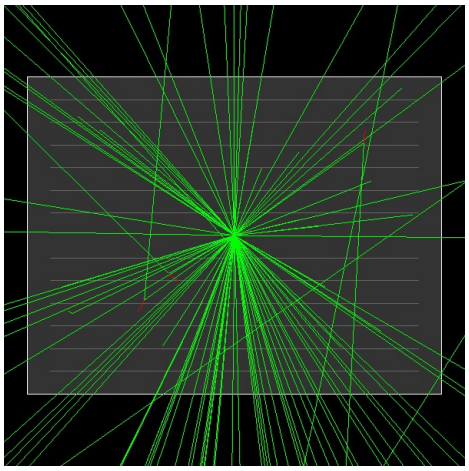 b) 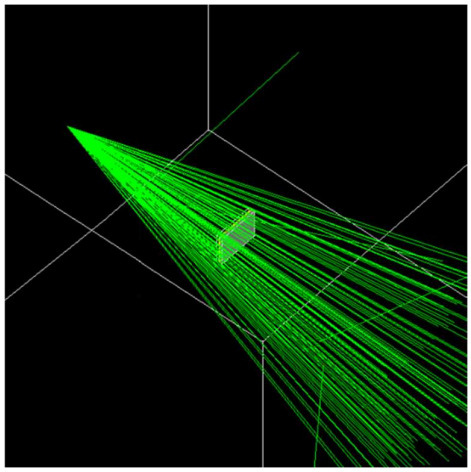

Figure 3.44. a) Front View of Simulated NEMA Phantom b) Simulated Gamma Photons 2.5 Meters from the Face of the Detector.

Small spherical source has 140 KeV positioned 2.5m far from SPECT head's center of FOV (Figure 3.44.b).

```
/gate/source/addSource                      GammaSource
/gate/source/GammaSource/gps/type           Volume
/gate/source/GammaSource/gps/shape          Sphere
/gate/source/GammaSource/gps/radius         0.125 mm
/gate/source/GammaSource/gps/centre         -250. 0. 0. cm
/gate/source/GammaSource/gps/particle       gamma
/gate/source/GammaSource/gps/energytype     Mono
/gate/source/GammaSource/gps/monoenergy     140. keV
/gate/source/GammaSource/setActivity        200000000. Bq
/gate/source/GammaSource/gps/angtype        iso
/gate/source/GammaSource/gps/mintheta       80. deg
/gate/source/GammaSource/gps/maxtheta       100. deg
/gate/source/GammaSource/gps/minphi         160. deg
/gate/source/GammaSource/gps/maxphi         190. deg
```

The source defined as isotropic but to increase the speed of simulation, the photons came directly to SPECT head taken into consideration for the imaging simulations. For this simulation 20 MBq of activity defined and simulation run during 10 seconds. In other words 2×10^9 photons transported. Total simulation took 41 hours with 4GHz processor.

The output folder with ASCII format has converted to use with MATLAB code. All the information in output folder are the photons inside the opened energy window. The gamma hits info is positioned of every row of output folder. All the events and their coordinates have read with using the Y and Z coordinates in rows. The measured pixel values of gamma camera used for the calculations; the hits recorded as pixels. Home made MATLAB code can be analyzed as following

```
fid = fopen('D:\Gate\Burak\Burak-
IntRes_Dig335mmEn95Singles.dat');
dataAll = textscan(fid, '%f %f %f %f %f %f %f %f %f %f %f
%f %f %f %f %f %f %s %s %s');
fclose(fid);

detectorHalfSize1 = 500/2;
detectorHalfSize2 = 600/2;
coordsDist(:,1)=dataAll{1,13}(:)+detectorHalfSize1;
coordsDist(:,2)=dataAll{1,14}(:)+detectorHalfSize2;

matSize = 1351;
pixelsize = 746/matSize;
im = zeros(matSize);

xPixel = zeros(length(coordsDist(:,1)),1);
yPixel = zeros(length(coordsDist(:,2)),1);

for i = 1:length(coordsDist(:,1))
    xPixel(i) = floor(coordsDist(i,1)/pixelsize)+1;
    yPixel(i) = floor(coordsDist(i,2)/pixelsize)+1;
    im(yPixel(i),xPixel(i)) = im(yPixel(i),xPixel(i))+1;
end

figure,imshow(im,[]);colorbar;impixelinfo
figure;plot(im(650,:));
```

Output of MATLAB code saved as DICOM format. Profiles created on to saved images and analyzed as described in section 3.2.

After each simulation the average FWHM values are determined from 13 slits. The measured FWHM values are plotted against the spatial blurring parameter. After that data points are fitted to a linear function. Using this function, the spatial blurring parameter for the FWHM value measured in Section 3.2.1 will be determined. After this determination, the simulation has run once more (25).

3.3.2. System Spatial Resolution Measurement Simulation for with and without Scatter

In this simulation, in addition to collimator, two line sources positioned at 10cm distance to collimator surface. For this purpose, firstly, capillary tubes has 1mm inner diameter, 6mm outer diameter defined (Figure 3.45). The blue box around the sources is filled with air for without scatter medium measurement, while filled with PMMA for with scatter medium measurement.

```
/gate/space/daughters/name Phantom1
/gate/space/daughters/insert cylinder
/gate/Phantom1/geometry/setRmax 3.  mm
```

```
/gate/Phantom1/geometry/setRmin 0.5 mm
/gate/Phantom1/geometry/setHeight 24. cm
/gate/Phantom1/placement/setTranslation -13.5 5. 0. cm
/gate/Phantom1/setMaterial Glass
/gate/Phantom1/vis/forceSolid
/gate/Phantom1/vis/setColor magenta

/gate/space/daughters/name Phantom2
/gate/space/daughters/insert cylinder
/gate/Phantom2/geometry/setRmax 3.  mm
/gate/Phantom2/geometry/setRmin 0.5 mm
/gate/Phantom2/geometry/setHeight 24. cm
/gate/Phantom2/placement/setTranslation -13.5 -5. 0. cm
/gate/Phantom2/setMaterial Glass
/gate/Phantom2/vis/forceSolid
/gate/Phantom2/vis/setColor magenta
```

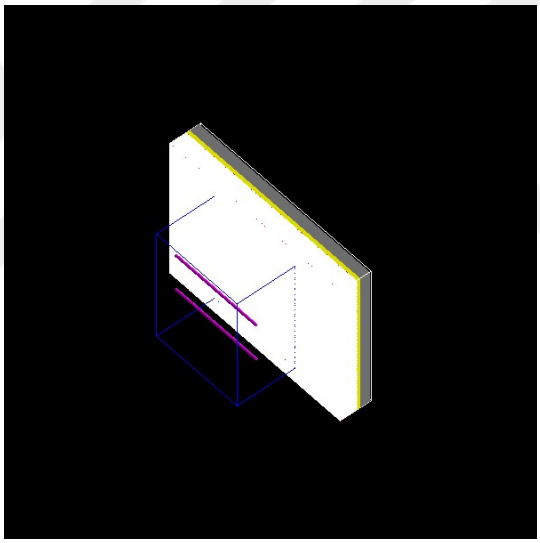

Figure 3.45. Simulation Setup for NEMA System Resolution

After the definition, Tc-99m source positioned inside the tubes. The source defined as isotropic but to increase the speed of simulation, the photons came directly to SPECT head taken into consideration for the imaging simulations. For this simulation 100 MBq of activity defined and simulation run during 10 seconds. In other words 2×10^9 photons transported. Total simulation took 43 hours with 4GHz processor.

```
/gate/source/addSource line_source
/gate/source/line_source/gps/type Volume
/gate/source/line_source/gps/shape Cylinder
/gate/source/line_source/gps/radius .5 mm
/gate/source/line_source/gps/halfz 12. cm
/gate/source/line_source/gps/centre -13.5 5. 0. cm
/gate/source/line_source/gps/particle gamma
```

```
/gate/source/line_source/gps/energy 140. keV
/gate/source/line_source/setActivity 100000000. Bq
/gate/source/line_source/gps/angtype iso
/gate/source/line_source/gps/mintheta 10. deg
/gate/source/line_source/gps/maxtheta 170. deg
/gate/source/line_source/gps/minphi   100. deg
/gate/source/line_source/gps/maxphi   260. Deg
```

Output of MATLAB code saved as DICOM format. Profiles created on to saved images and analyzed as described in section 3.3.1 (25).

3.3.3. System Planar Sensitivity

First of all a source has 2 mm thickness, 15 cm diameter positioned 10 cm distance from collimator face and the source centered in FOV. To calculate sensitivity, Tc-99m defined which decays over time. To define Tc-99m below physical process added to code.

```
/gate/physics/addProcess RadioactiveDecay
```

Source defined afterwords with below code

```
/gate/source/addSource                tc99m
/gate/source/tc99m/setActivity        5000000. Bq
/gate/source/tc99m/gps/particle ion
/gate/source/tc99m/gps/ion            43 99 0 142.6832
/gate/source/tc99m/gps/energytype     Mono
/gate/source/tc99m/gps/monoenergy     0. MeV
/gate/source/tc99m/setForcedUnstableFlag   true
/gate/source/tc99m/setForcedHalfLife  21624.129 s
/gate/source/tc99m/gps/type Volume
/gate/source/tc99m/gps/shape Cylinder
/gate/source/tc99m/gps/radius 7.5 cm
/gate/source/tc99m/gps/halfz 1. mm
/gate/source/tc99m/gps/centre -13.6 0. 0. cm
/gate/source/tc99m/gps/posrot1 0. 0. -1.
/gate/source/tc99m/gps/posrot2 0. 1. 0.
/gate/source/tc99m/gps/angtype iso
```

Simulation continued during 100 seconds with 5 MBq and took 50 hours with 4Ghz processor (25).

4. RESULTS

After the NEMA acquisitions with gamma camera and the calculations with Gate Monte Carlo Simulation, the acquired data for each type of measurements calculated with the given NEMA formulas, described in Section 3.

4.1. Intrinsic Spatial Resolution Results

As described in Section 3.2.1, intrinsic spatial resolution measured with gamma camera and simulated with Gate and results are indicated in Table 4.1.

Table 4.1. Intrinsic Spatial Resolution Results

Measured value	UFOV	CFOV
FWHM (mm)	3.595	3.601
FWTM (mm)	6.553	6.563

Intrinsic spatial resolution calculated with Gate simulation. To have accurate calculation which is close value to gamma camera value, different blurring factors applied, and intrinsic resolution FWHM values of gamma camera calculated. After having the closest value of FWHM to gamma camera calculation, that blurring factor applied for every Gate simulation.

Applied blurring factors can be analyzed in Table 4.2

Table 4.2. Applied Blurring Factors and Calculated FWHM Values with Gate

Spatial blurring factor	FWHM (mm)
2.0	2.271
2.5	2.748
3.0	3.241
3.5	3.744
4.0	4.244

This calculation has let to know the value to be set for the blurring value which is 3.35. After the setup of this value, another intrinsic spatial resolution test simulated with Gate and the calculated value for FWHM was 3.585 as seen in Figure 4.1.

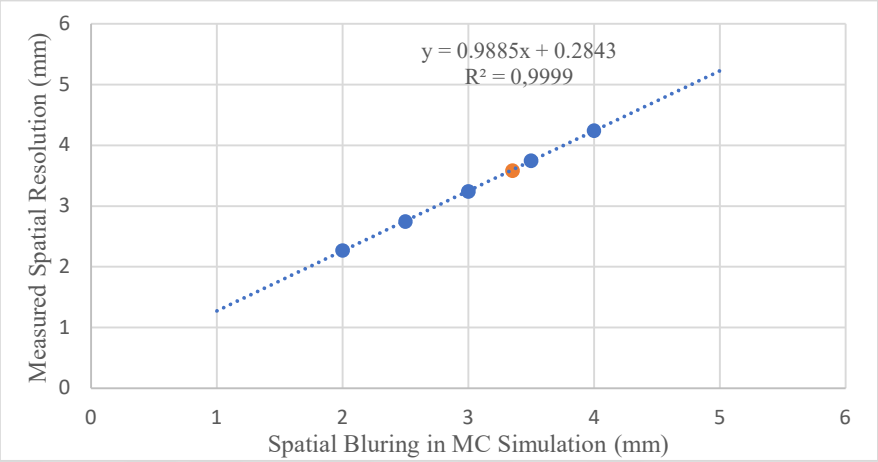

Figure 4.1. Graph Spatial Blurring Over Measured Spatial Resolution

As result the measured FWHM value is 3.595 and in Monte Carlo simulation FWHM value is 3.585. The difference between two values is less than 0.3%.

4.2. Intrinsic Count Rate Performance in Air (Copper Plates Method)

Following values calculated for the intrinsic count rate with the specified NEMA formulas described in section 3.2.2. You can observe the result in Table 4.3

Table 4.3. Measured Intrinsic Count Rate Values

Removed copper plates	Time difference from previous scan	Ki (Total count)	Ci (Background corrected count rate)	OCRi (Observed count rate)	ICRi (Initial count rate)	ICRi×0.8(20% loss of initial count rate)
1	0	25222	5322.6	0.27	0.27	0.21
2	35	31464	11564.6	0.58	0.44	0.35
3	71	37908	18008.6	0.90	0.72	0.58
4	105	49861	29961.6	1.50	1.19	0,96
5	139	69877	49977.6	2.50	1.97	1.58
6	171	103017	83117.6	4.16	3.25	2.60
7	222	155487	135587.6	6.78	5.36	4.29
8	260	248171	228271.6	11.42	8.84	7.08
9	293	396089	376189.6	18.82	14.59	11.67
10	328	629537	609637.6	30.49	24.06	19.25
11	363	996115	976215.6	48.83	39.70	31.76
12	398	1526349	1506450	75.35	65.48	52.38
13	431	2219323	2199424	110.01	108.01	86.41
14	467	2907560	2887661	144.43	178.17	142.53
15	500	3067039	3047140	152.41	293.90	235.12
16	544	1915731	1895832	94.82	484.80	387.84
17	580	370503	350603.6	17.54	799.69	639.76

From the input values, C_i: Back round corrected total count, K_i: Total count, R_{bkg}: Back round count rate, Δt_i : Scan time in seconds, OCRi. Observed count rate, ICRi: Initial count rate and ICRi×0,8: 20% loss of ICRi vales calculated (Table 4.3).

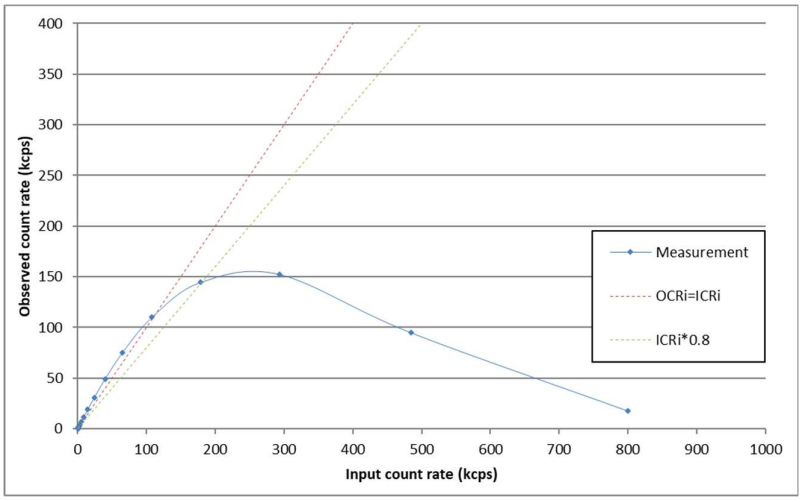

Figure 4.2. Plot Input Count Rate Over Observed Count Rate

From the measurements Maximum obtained count rate measured as 153.5 kcps, observed count rate at 20% loss measured as 145.2 kcps. Gained count rate versus the input count rate graph can be seen in Figure 4.2.

4.3. System Planar Sensitivity and Collimator Penetration and Scatter

System planar sensitivity and collimator penetration fraction (PF) tests measured with gamma camera for both LEHR and LEHRS collimators. Both values simulated as described in section 3.3.3. Planar sensitivity and penetration fraction values reported with the related NEMA formulas as described in section 3.2.3.

For LEHR collimator, static acquisitions from given distances (10, 20, 50, 100, 150, 200, 250 mm) acquired with $A_{cal} = 5{,}1\ mci = 188.7 MBq$. Total counts, decay corrected counts and duration of acquisition have taken into consideration for penetration fraction calculation and recorded can be indicated in Table 4.4.

Table 4.4. System Planar Sensitivity and Penetration Fraction Measurements

Distance (mm)	Duration (second)	Total count	Ri (decay corrected total count)
10	269.31	1584666	5909.54
20	271.63	1581098	5846.09
50	273.93	1563939	5734.20
100	275.75	1542546	5618.66
150	278.77	1531686	5518.66
200	282.74	1527650	5427.41
250	286.58	1523143	5339.27

System planar sensitivity measured from the values acquired at 100 mm as 77,21 cps/MBq for LEHR collimator.

For penetration fraction, the plot created distance versus Ri and this graph fitted to an exponential decay function as described in Section 3.2.3. The graph can be observed in Figure 4.3.

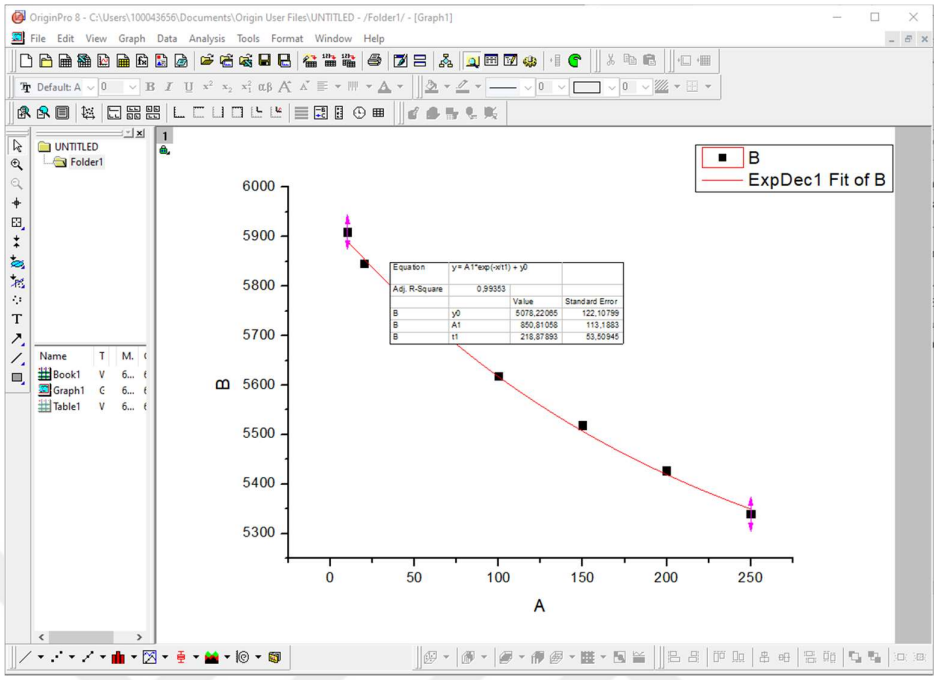

Figure 4.3. Curve Fitting for LEHR Penetration Fraction

For LEHRS collimator, static acquisitions from given distances (10, 20, 50, 100, 150, 200, 250 mm) acquired with $A_{cal} = 6{,}63\ mci = 245{,}31\ MBq$. Total counts, decay corrected counts and duration of acquisition have taken into consideration for penetration fraction calculation and recorded can be observed in Table 4.5.

Table 4.5. System Planar Sensitivity and Penetration Fraction Measurement Results

Distance (mm)	Duration (second)	Total count	Ri (decay corrected total count)
10	207.25	1402259	6788.29
20	209.03	1397096	6705.89
50	210.67	1376846	6557.58
100	213.16	1350034	6354.82
150	215.71	1338656	6227.20
200	218.67	1333497	6119.49
250	222.79	1330861	5994.82

System planar sensitivity measured from the values acquired at 100 mm as 76,75 cps/MBq for LEHRS collimator.

For penetration fraction, the plot created distance versus Ri and this graph fitted to an exponential decay function as described in Section 3.2.3. The graph can be observed in Figure 4.4.

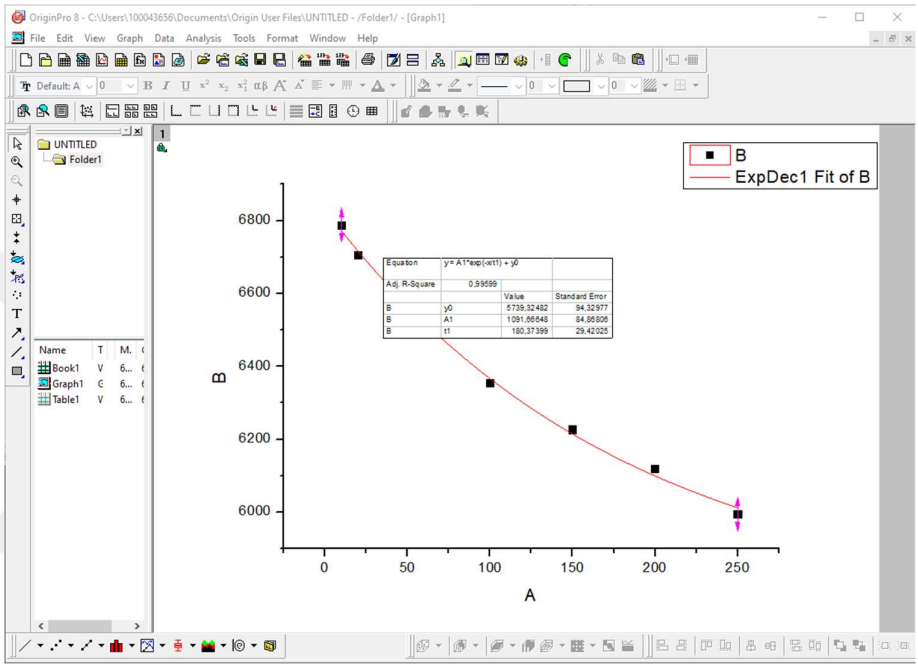

Figure 4.4. Curve Fitting for LEHRS Penetration Fraction

After curve fitting, data points collected, and the penetration fraction formula applied.

Same sensitivity calculation done for both LEHR and LEHRS collimator with Gate as described in Section 3.3.3. and you can see the results in Table 4.6.

Table 4.6. LEHR and LEHRS Collimators Sensitivity Results

	Manufacturer's specification	Measured (cps/MBq)	MC Simulation (cps/MBq)	Difference between measurement and simulation (%)
LEHR	72	77.21	80.53	4.12
LEHRS	92	76.75	99.9	23.17
LEHR/LEHRS	0.78	1.01	0.81	

Penetration fraction calculated as 0,084 for LEHR collimator.

Penetration fraction calculated as 0,082 for LEHRS collimator.

4.4. System Spatial Resolution without Scatter

The needed setup completed and assessed for both LEHR and LEHRS collimators with gamma camera and Gate simulation as described in section 3.2.4 and 3.3.2

Table 4.7. System Spatial Resolution without Scatter Results

	Manufacurer's specification (mm)	Measured FWHM (mm)	MC Simulation FWHM (mm)	Difference between measurement and simulation (%)
LEHR	7.40	7.36	6.91	6.16
LEHRS	7.40	7.59	7.21	5.05
LEHR/LEHRS	1.00	0.96	0.96	

4.5. System Spatial Resolution with Scatter

Measurement for the mentioned test assessed for both LEHR and LEHRS collimators with gamma camera and Gate simulation as described in section 3.2.5 and 3.3.2.

Table 4.8. System Spatial Resolution with Scatter Results

	Manufacurer's specification (mm)	Measured FWHM (mm)	MC Simulation FWHM (mm)	Difference between measurement and simulation (%)
LEHR	NA	7.99	7.51	6.01
LEHRS	NA	8.46	8.04	5.21
LEHR/LEHRS	NA	0.94	0.93	

4.6. SPECT Reconstructed Spatial Resolution without Scatter

This test for both LEHR and LEHRS collimators measured and calculated with the methods described in Section 3.2.6.

The measurement results for LEHR and LEHRS collimators can be observed in Table 4.9 and Table 4.10, in order.

Table 4.9. SPECT Reconstructed Spatial Resolution Measurements (in mm) for LEHR Collimator

Central Point				
Trans	Xc,t	10.70	Yc,t	10.71
Sag	Yc,s	10.79	Zc,s	11.26
Cor	Xc,c	10.80	Zc,c	11.05
Peripheral Point Left				
Trans	Xpl,t	10.57	Ypl,t	9.63
Sag	Ypl,s	10.03	Zpl,s	10.12
Cor	Xpl,c	10.42	Zpl,c	9.63
Peripheral Point Right				
Trans	Xpr,t	10.98	Ypr,t	9.34
Sag	Ypr,s	10.13	Zpr,s	9.86
Cor	Xpr,c	10.63	Zpr,c	9.27

Table 4.10. SPECT Reconstructed Spatial Resolution Measurements for LEHRS Collimator

Central Point				
Trans	Xc,t	11.22	Yc,t	10.95
Sag	Yc,s	10.80	Zc,s	10.48
Cor	Xc,c	10.78	Zc,c	10.06
Peripheral Point Left				
Trans	Xpl,t	11.16	Ypl,t	9.49
Sag	Ypl,s	10.26	Zpl,s	9.88
Cor	Xpl,c	10.75	Zpl,c	9.36
Peripheral Point Right				
Trans	Xpr,t	11.08	Ypr,t	9.56
Sag	Ypr,s	9.96	Zpr,s	10.30
Cor	Xpr,c	11.23	Zpr,c	9.57

After the measurements the SPECT spatial resolution without scatter assessed. The results can be seen in Table 4.11 for both collimators.

Table 4.11. SPECT Spatial Resolution Values for LEHR&LEHRS Collimators

	LEHR	LEHRS	Difference (%)
Central Transaxial (mm):	10.76	10.94	-1.67
Central Axial (mm):	11.16	11.06	0.90
Peripheral Radial(mm):	10.65	10.28	3.47
Peripheral Tangential (mm):	9.79	9.82	-0.31
Peripheral Axial (mm):	9.72	9.78	-0.60

4.7. SPECT Reconstructed Spatial Resolution with Scatter

SPECT reconstructed spatial resolution with scatter calculated from three line resources in a cylinder and results calculated for both LEHR and LEHRS collimator as described in Section 3.2.7. Measurements done from transaxial plane.

Measurement results for LEHR and LEHRS collimators can be observed in Table 4.12 and Table 4.13, respectively.

Table 4.12. SPECT Reconstructed Spatial Resolution with Scatter Measurements for LEHR Collimator

Center	Transaxial	Xc,t	11.19	Yc,t	10.70
Up	Transaxial	Xpl,t	12.80	Ypl,t	9.17
Right	Transaxial	Xpr,t	8.69	Ypr,t	12.56

Table 4.13. SPECT Restructured Spatial Resolution with Scatter Measurements for LEHRS Collimator

Center	Transaxial	Xc,t	11.38	Yc,t	11.38
Up	Transaxial	Xpl,t	8.39	Ypl,t	10.99
Right	Transaxial	Xpr,t	11.34	Ypr,t	8.66

After the measurements reconstructed spatial resolution with scatter calculated for both collimators. Measurement results can be observed in Table 4.14.

Table 4.14. SPECT Reconstructed Spatial Resolution with Scatter Values for LEHR and LEHRS Collimators.

	LEHR	LEHRS	Difference
Central (mm):	10.95	11.38	-3.92
Tangential (mm):	8.92	8.52	4.48
Radial (mm):	12.68	11.16	11.94

4.8. System Volume Sensitivity

System volume sensitivity (SVS) assessed and average volume sensitivity per axial centimeter (VSAC) calculated for both LEHR and LEHRS collimators as described in Section 3.2.8.

It is shown that system volume sensitivity and average volume sensitivity per axial centimeter for LEHR collimator in Table 4.15.

Table 4.15. SVS and VSAC Calculation for LEHR Collimator

Total Count:	44268897
Total Duration (s):	1383
Activity (mCi):	15.41
Activity (MBq):	570.17
Activity Measurement time:	17:58:00
Acquisition start:	18:16:44
Halfway duration:	0.0081
Halfway Time:	18:28:16
Decay.Corrected.Activity. (MBq):	549.98
Volume (cc):	6381.10
Activitiy consantration. (MBq/cc):	0.0862
SVS (cps/MBq/cc):	371388.92
VSAC:	19967.14

System volume sensitivity and average volume sensitivity per axial centimeter for LEHRS collimator can be observed in Table 4.16.

Table 4.16. SVS and VSAC Calculation for LEHRS Collimator

Total Count:	44606031
Total Duration (s):	1383
Activity (mCi):	14.35
Activity (MBq):	530.95
Activity Measurement time:	19:25:00
Acquisition start:	19:42:05
Halfway duration:	0.0081
Halfway Time:	19:53:36
Decay.Corrected.Activity. (MBq):	513.77
Volume (cc):	6381.10
Activitiy consantration. (MBq/cc):	0.081
SVS (cps/MBq/cc):	400585.41
VSAC:	21536.85

5. CONCLUSION AND DISCUSSION

Gamma camera systems form an important part of functional imaging in nuclear medicine. At the stage of purchasing a gamma camera, hospitals can compare the devices of different manufacturers by looking at the NEMA specifications provided by the manufacturers and select the system that suits their needs. Checking the physical parameters is esential to compare the specifications of device and lets the department to understand the most important specifications to control. In order to ensure that the same image quality parameter is tested in the same way in each device, NEMA has established rules on how and with, the equipments to be used for pecific measurement and how the obtained data will be analyzed. (24). Those rules well defined in the NEMA guideline for gamma camera performance tests.

Imaging cannot be applied with a gamma camera without initating a collimator. A gamma camera system in a hospital has different collimators for different purposes. First of all, the collimator suitable for the isotope energy to be used should be selected (for example, low energy for Tc99m). Secondly, HR (high resolution), general purpose, high sensitivity collimators are selected depending on whether high resolution or high sensitivity is desired in imaging. Generally, the user has to choose between high sensitivity and high resolution power. The sensitivity is low in high resolution collimator, and the resolution is low in high sensitivity collimator. Choosing the correct collimator pair for corresponding examination gives the aimed best image quality to doctors and technologists.

In this thesis, it is aimed to compare the image quality parameters of a collimator, which a gamma camera manufacturer claims to increase the sensitivity without resolution loss, with a collimator with high resolution power according to the NEMA standard. For this purpose, tests were carried out on the selected tests in the NEMA NU-1 document on both collimators in the same gamma camera system. Image quality parameters are compared. In order to rule out performance deficiencies that may arise from possible measurement and production errors, the gamma camera system was simulated in the gate-mounted card code with the collimator. And some tests have also been made with simulation simulation over selected parameters. For Gate monte carlo simulation, the intrinsic spatial resolution and energy resolution of the gamma camera must be evaluated. In the system, these parameters were measured according to the NEMA method, and the intrinsic spatial resolution is 3.595 mm at UFOV and the intrinsic energy resolution is

9.5% at 140 keV. Both values are equal to or better than manufacturer specifications. The intrinsic energy resolution parameter is set directly in the simulation. However, NEMA resolution phantom was simulated to determine the spatial blurring parameter that will give the measured intrinsic spatial resolution. The spatial blurring parameter was changed between 2.0-4.0 and the blurring parameter was determined as 3.35, which is suitable for the real state of the gamma camera, and the simulation was run once again at this value. As a result of this simulation, the intrinsic separation power was measured as 3.585 mm, and it was determined that the difference with the real situation was less than 0.3%. This result shows us that the gamma camera simulation in this thesis study is reliable enough. In order to add the dead time characteristics of the gamma camera to the simulation, intrinsic count rate performance tests were also carried out. According to the measurement result, the maximum observed count rate was measured as 153.5 kcps for 140 kev and 20% energy window. Since the manufacturer's specification for this parameter could not be found, it could not be compared. The dead time characteristic model has not been added, since no simulations that require high counting speed are performed in Monte Carlo simulations.

System planar sensitivity values were measured as 77.21 cps/MBq and 76.75 cps/MBq for LEHR and LEHRS collimators, respectively. Manufacturer specifications for these collimators are given as 72 and 92 cps/MBq, respectively. It has been determined that the LEHR collimator meets the manufacturer's specification, but the LEHRS collimator does not reach the value specified in the manufacturer's catalogue. In the Monte Carlo simulation, the same values were calculated as 80.53 and 99.90 cps/MBq. While the difference between the measured and calculated values for the LEHR collimator is less than 5%, this difference is 23% for the LEHRS. Considering the sensitivity ratios of both collimators, although the manufacturer's specification and Monte carlo results are in agreement, this ratio is much higher than expected in the measurement results. For the LEHRS collimator, the measured sensitivity value was significantly lower than both the company specification and the monte carlo simulation, suggesting that there may be a manufacturing defect in the collimator used during the measurements.

Penetration fractions for LEHR and LEHRS collimators were measured as 0.084 and 0.082, respectively. The manufacturer's specification for the penetration fraction could not be found, so it could not be compared. However, as with planar sensitivity, the fact that the planar sensitivity of both collimators is very close to each other suggests that there may be a production problem in the collimator. The manufacturer's data for System

spatial resolution is 7.4 mm for both collimators, while 7.36 and 7.59 for the LEHR and LEHRS collimators, respectively. The LEHRS collimator does not meet the manufacturer's specification. In the Monte Carlo simulation, the same values were calculated as 6.91 and 7.21. While the FWHM ratios of both collimators are similar for measurement and Monte Carlo simulations, the different things between the calculated and simulated FWHM values of each collimator are slightly larger than 5%. The reason for this is thought to be structures such as collimator cover, touchpad sensor, which may cause an increase in the source detector distance during physical measurements. Similar results were obtained in the measurements made in the scattering medium.

In SPECT spatial resolution measurements performed without scattering medium, similar measurement results were obtained for both collimators (Table 4.11). It was found that planar spatial separation power differences were not reflected in the SPECT resolution. It is thought that the reason for this is that the FBP method creates a certain blurring in the cross-sectional images during the reconstruction phase and therefore the resolution differences of the collimators are eliminated during the reconstruction phase. SPECT tests could not be simulated in Monte Carlo. Therefore, a comparison could not be made. Similar results were observed in the SPECT spatial resolution tests performed in the scattering medium.

In the final system volume sensitivity test, approximately 8% higher sensitivity was obtained in the LEHRS collimator compared to the LEHR collimator. In this thesis study, in which a medical device manufacturer's collimators named LEHR and LEHRS were compared with both NEMA methods and Monte carlo simulation method, the measurement results mostly did not support the simulation results. As discussed above, it was thought that the reason for this was mainly the errors in the collimator production. In this thesis, experience has been gained in the application of NEMA tests, as well as gains in the application of the monte carlo method to gamma camera simulation. Again, this thesis study also reveals the importance of testing the compliance of the production specifications by passing the acceptance test in medical devices taken to a hospital. To run those tests, NEMA method defines the finest methods to evaluate gamma camera performance.

6. REFERENCES

1. Celler A., Rova A., Hamarneh G., Development of NEMA based Software for Gamma Camera Quality Control *J Digit Imaging.* 2008 p.243–255.

2. U. Raft, V.M. Spitzer, W.R. Hendee, Practicality of NEMA Performance Specification Measurements for User-Based Acceptance Testing and Routine Quality Assurance, *J. nucl Med* 1984 p.679-687.

3. G Santin, D Strul, S Staelens et al. GATE: a simulation toolkit for PET and SPECT *Phys Med Biol*. 2004 p.49-61.

4. Alhamad K., Monte Carlo Simulation of a Curved-Detector Gamma Camera Aberdeen, University of Aberdeen, 2020.

5. Ganguly D., Medical Imaging *Communications in Computer and Information Science* Springer, Boston, 2002.

6. Iniewski K., *Medical Imaging Principles, Detectors, and Electronics* New Jersey: John Willey & Sons, Inc., Publication, 2009

7. Wagner H.N., Szabo Z., Buchanan W., *Principles of Nuclear Medicine,* 3rd edition, W. B. Saunders, Philadelphia, 1995.

8. Wernick M.N., Aarsvold J.N., *Emission Tomography, The Fundamentals of PET and SPECT*, Elsevier, Academic Press, Amsterdam, Boston, 2004.

9. Rahmim A., Zaidi H., PET versus SPECT: Strengths, limitations and challenges, *Nucl. Med. Commun. 29*, 2008, p. 193–207.

10. Biersack H.J., Freeman L.M., *Clinical Nuclear Medicine* Springer-Verlag Berlin Heidelberg, New York, 2007

11. Wernick M.N., Aarsvold J.N., *Emission Tomography, The Fundamentals of PET and SPECT*, Elsevier, Academic Press, Amsterdam, Boston, 2004.

12. https://www.hopkinsmedicine.org/health/treatment-tests-and-therapies/positron-emission-tomography-pet

13. Khalil M.M, *Basic sciences of Nuclear Medicine*, Springer Verlag Heidelberg Dordrecht London, New York, 2011.

14. Zaidi H., *Quantitative Analysis in Nuclear Medicine Imaging*, Springer, Berlin, 2006.

15. Lau Y.H., Hutton B.F., Beekman F.J. Choice of colli mator for cardiac SPECT when resolution compensation is included in iterative reconstruction. *Eur J Nucl Med 28 (1)*: 2008, p.39-47.

16. Inoue Y., Shirouzu I., Machida T., et al. Physical characteristics of low and medium energy collimators for 123-I imaging and simultaneous dual iso tope imaging. *Nucl Med Commun 24(11)* 2003, p.1195-1202.

17. Accorsi R., Brain single photon emission CT physics principles. *Am J. Neuroradiol 29(7)* 2008, p.1247-1256.

18. Peremans K., Cornelissen B., Van Den Bossche B., et al. A review of small animal imaging planar and pinhole SPECT gamma camera imaging. *Vet Radiol Ultrasound 46(2)* (2005) p.162-170.

19. Harbert J.C., Eckelman W.C., Neumann R.D. *Nuclear Medicine Diagnosis and Therapy*. Thieme Medical, New York, 1996.

20. Powsner R.A., Powsner E.R., *Esential Nuclear Medicine Physics*, 2nd ed. Blackwell Publishing Ltd. Oxford, 2006.

21. Shapiro J. *Radiation Protection A Guide for Scientists, Regulators, and Physicians,* 4th Edition, Harvard University Press, Cambridge MA, 2002.

22. https://www.investopedia.com/terms/m/montecarlosimulation

23. https://opengate.readthedocs.io/en/latest/introduction.html#overview

24. National Electrical Manufacturers Association*, NEMA Standards Publication NU 1-2012 Performance Measurements of Gamma Cameras* Rosslyn, 2013.

25. Open Gate Collaboration, *Gate user guides V6.0,* Lyon, 2006.

APPENDIX.A Radiology Imaging Modalities

X-ray Imaging (Radiography)

Medical radiography is a broad word that encompasses a variety of studies that demand the use of x-ray techniques to investigate the inner organs of the body. With the aim of this page, radiography refers to a method to produce and record an x-ray pattern in order to give the user a static image (or images) when the exposure is over. It differs from other imaging techniques like computed tomography, computed radiography, and fluoroscopy. Radiation therapy treatment planning may also involve the use of radiography.

By taking pictures of the body's internal structure and analyzing them for signs of disease, foreign objects, structural damage, or anomalies, it can be used to diagnose or treat patients.

A radiographic procedure involves passing an x-ray beam inside the body. The interior form scatters or absorbs some of the x-rays, but the remaining pattern is passed to a detector in which it can be captured as an image for subsequent analysis. Recoding the pattern may take place electronically or on film.

When a record of a static image is sought, radiography is employed in many different sorts of examinations and operations. Several instances demand:

- Dental examination
- Verification of correct placement of surgical markers prior to invasive procedures
- Mammography
- Orthopedic evaluations
- Spot film or static recording during fluoroscopy
- Chiropractic examinations

Electromagnetic waves are a category of radiation that includes X-rays (having wavelengths between 0.01 to 10 nanometers). Applying X-ray imaging, your body's interior could be visualized. The images reflect the various body parts in various shades of black and white. That is why various tissues absorb radiation in a wide range of methods. As calcium in bones absorbs the most x-rays, bones appear white. Other soft tissues -fat absorb less blood - appear grey. Lungs seem black owing to the least air absorbing.

In many cases, radiography is essential for evaluating the body's diverse osseous

structures. as for determining the kind and size of a fracture. With the use of contrast, it is also feasible to evaluate the lungs, as well as other soft tissue organs of the body like the uterus and gastrointestinal tract. Stereotactic breast biopsies, intra-articular steroid injections, and catheter angiography are just a few of the treatments that can be performed with the use of radiography. A number of illnesses, involving as fractures, different types of pneumonia, cancers, and congenital anatomic anomalies, can be assessed with radiography regarding the visualization and study of opacities on a radiograph, radiographic interpretation.

Computed Tomography (CT)

The noninvasive medical treatment known as computed tomography (CT), sometimes called as "computerized tomography" or "computed axial tomography" (CAT), creates cross-sectional figures of the body utilizing specialized X-ray equipment. Similar to the slices in a loaf of bread, each cross-sectional image shows a "slice" of the individual being photographed. There are numerous diagnostic and therapeutic uses for these cross-sectional pictures.

Every part of the body can get a CT scan for numerous aims (e.g., diagnostic, treatment planning, interventional, or screening). The majority of CT scans are done as outpatient surgeries.

How a CT system functions; the patient is moved by a motorized table by the help of a spherical CT imaging system opening.

An X-ray source and a detection assembly within the system circle around the patient while the patient is inside the opening. Typically, one revolution takes one second or less. A portion of the patient's body is passed through by a narrow, fan-shaped X-ray beam produced by the rotating X-ray source.

The X-rays that pass through the patient's body are registered by detectors in rows across from the X-ray source as a snapshot during the image-creation process. During a full rotation, several "snapshots" (taken from various angles through the patient) are gathered.

The picture data are transferred to a computer to be reconstructed into one or more cross-sectional images (slices) of the internal organs and tissues for each rotation of the X-ray source and detector assembly.

Compared to traditional X-ray images, such a chest X-Ray, CT images of internal organs, bones, soft tissue, and blood arteries offer higher clarity and detail.

CT is a useful medical technology that can assist a doctor in:

- Identify a disease, injury, or abnormality
- Coordinate and direct therapeutic or interventional operations
- Evaluate the efficacy of therapy (e.g., cancer treatment)
-

Rewards & Risks; when performed properly, a CT scan has far more advantages than disadvantages. When employed to diagnose, plan therapy for, and assess a variety of illnesses in both adults and children, CT scans can offer detailed information. Additionally, exploratory surgery might not be necessary given the comprehensive images produced by CT scans.

Ionizing radiation hazards and potential adverse effects from the intravenous contrast agent, or dye and it is possible to be used to go up visibility, are two issues with CT scans. A person's lifetime chance of acquiring cancer may somewhat rise as a result of exposure to ionizing radiation. Because younger patients have a higher cancer risk per unit dose of ionizing radiation than adults and because the effects of radiation exposure take longer for younger patients to develop as cancer, exposure to ionizing radiation is seriously affecting in pediatric patients.

However, when we compare it with the benefit of an appropriate diagnosis or intervention, the risk of a medically essential imaging exam is fairly low in both children and adults. It is crucial to use the proper exposure factors when performing CT scans on children since using exposure settings intended for adults may result in a higher radiation dose than is necessary to create a meaningful image for a pediatric patient.

Every part of the body can get a CT scan for a numerous aims (e.g., diagnostic, treatment planning, interventional, or screening). The majority of CT scans are done as outpatient surgeries. Since it was created at a research division of EMI, a firm best known today for its music and recording business, computed tomography was first referred to as the "EMI scan." Later, it was referred to as body section radiography and computerized axial tomography (CAT or CT scan).

Instead of collecting a sequence of images of distinct body slices like the first CT scanners did, the majority of current CT machines take continuous images in a helical (or spiral) pattern. Helical CT is faster than prior CT methods, creates better 3-D images of body regions, and may be better able to detect minor abnormalities. The most recent CT scanners, also known as multi slice CT or multidetector CT scanners, enable the imaging

of more slices in less time.

A vast collection of two-dimensional X-ray images captured around a single axis of rotation are combined with digital geometry processing to create a three-dimensional image of the interior of an item. Through a technique called "windowing," CT produces a large amount of data that can be changed to show different anatomical structures relied on their capacity to deflect the X-ray / Rontgen beam. Modern scanners lead this amount of data to be reconstructed in multiple planes or even as volumetric (3D) reconstructed structures, whereas historically the images produced were in the axial or transverse plane, orthogonal to the long axis of the body.

A contrast (imaging) agent, also known as a "dye," may occasionally be used during a CT scan. Before the procedure, the dye may be administered orally, intravenously, intravenously by enema, or in a combination of all three modalities. The contrast dye makes some inside body regions stand out, giving images greater clarity. Two dyes that are frequently used in CT are barium and iodine.

Magnetic Resonance Imaging (MRI)

A non-invasive imaging method named magnetic resonance imaging constructs three-dimensional, intricate anatomical images. In terms of diagnosis, and monitoring the therapy, this method frequently is employed. Moreover, with the cutting-edge technology, it stimulates and identifies changes in the rotational axis of protons in the water providing alive tissues for detection of disease. At the same time, Protons placed in the body are obliged to align with the magnetic area formed by the powerful magnets used in MRI machines. The protons are initiated and spin out of equilibrium when a radiofrequency current is pulsed via the patient, and it leads them to challenge against the magnetic area. The energy obtained as the protons realign with the magnetic field can be identified by means of the MRI sensors when the radiofrequency field is turned off. How long it pursue for the protons to realign with the magnetic field is affected by how much energy is released. The surroundings and the chemical make-up of the molecules is relied on these magnetic characteristics and doctors can discriminate different types of tissues. A patient is positioned inside a huge magnet to create an MRI image, and extreme stillness throughout the imaging process to inhibit image blurring it must be sustained. Before or during the MRI, a patient might get intravenous contrast agents (typically involving the element gadolinium) to fasten the rate at which protons realign with the magnetic field. Following that the image is getting brighter as the protons realign more quickly.

MRI scanners are specially well originated to observe and image the body's soft tissues or non-bony portions. They are suggested that to be far from computed tomography (CT) and x-rays are not utilized because of dangerous ionizing radiation. With quite clearer view of the brain, spinal cord, and nerves are obtained with MRI rather than conventional x-rays and computed tomography (CT), which is applied for knee and shoulder injuries.

Aneurysms and tumors can also be identified with MRI, which can also divide between white matter and grey matter in the brain. When frequent imaging is demanded for diagnosis or therapy, particularly in the brain, MRI is the imaging modality of option since it does not apply x-rays or other radiation. However MRI is more expensive than CT scanning or x-ray imaging.

Functional Magnetic Resonance Imaging is one type of specialized MRI (fMRI.) This is initiated to observe brain architecture and find out which parts of the brain "activate" (use more oxygen) when performing different kinds of cognitive tasks. It suggests a potential new standard for evaluating neurological health and risk for neurosurgery and is used to raise our understanding of how the brain is organized.

Water molecules, built by hydrogen and oxygen atoms cover the majority of human body tissue.

Each hydrogen atom even with a smaller particle has a proton in its center. Due to resembling small magnets, protons are suggested to be highly sensitive to magnetic fields.

The way of pulling a compass's needle resembles the protons in body in the same order with the same direction, on lying under the strong scanner magnets.

The protons are then thrown out of alignment by short radio wave bursts that are subsequently directed towards certain parts of the body.

The protons realign when the radio waves are switched off. Receivers choose the radio signals that are absorbed as a result.

The precise position of the protons within the body is revealed by these signals.

As the protons in various forms of tissue realign at different speeds and emit different signals, they help differentiating between the many types of tissue in the body.

The signals obtained from the millions of protons in the body are connected to create a detailed image of the inside of the body, much as how millions of pixels on a computer screen might produce intricate visuals.

APPENDIX.B. Radiopharmacy

Basics of Nuclear Medicine Radiopharmaceuticals

A radiopharmaceutical is a radioactive substance made up of a pharmaceutical and a radionuclide that is used to diagnose and treat human ailments. As legend drugs, all radiopharmaceuticals are governed by the same laws as other medications. A radiochemical is different from a radiopharmaceutical in that the former cannot be delivered to humans since it may not be sterile and nonpyrogenic; any substance given to people must be sterile and nonpyrogenic. A radiopharmaceutical can be a labelled substance like 99mTc-tagged compounds or a radioactive element like 133Xe. Only around 5% of the radiopharmaceuticals used in nuclear medicine are employed for therapeutic effects; the majority, approximately 95%, are used for medical diagnostics. A appropriate pharmaceutical is selected when creating a radiopharmaceutical based on its preferential localization in a specific organ or its involvement in the physiological function of the organ. After that, a suitable radionuclide is attached to the medication of choice before being given to the patient. An external radiation detector can measure the radiation emitted from the organ to evaluate its morphological makeup and physiological operation. Since radiopharmaceuticals are often supplied in tracer quantities, they typically have little pharmacological impact. They essentially do not demonstrate a dosage response relationship. But in the case of therapeutic radiopharmaceuticals, it is the radiation itself, not the drug, that has the biological action that is seen. Both planar and tomographic imaging (also known as single-photon emission computed tomography, or SPECT), which depend on single-photon emitters, are possibilities for image acquisition in nuclear medicine operations. The other form is called positron emission tomography (PET), and it uses positron-electron annihilation to release two opposing photons that are 180 feet apart as part of its detecting procedure. The diversity and capability of their contrast agents to) respond to a clinical inquiry is the essential feature that sets these approaches apart from other modalities. In nuclear medicine, contrast agents are radiolabeled substances or radiopharmaceuticals that, when injected into the area of interest, emit vital data on the pathophysiologic state of the involved tissue. Both imaging methods are highly sensitive to molecular concentrations in the pico or nano range and have well-defined roles in molecular or functional imaging. The use of SPECT and PET radiopharmaceuticals is widely accepted in the fields of molecular imaging, biological research, and pharmaceutical development. But many SPECT tracers are FDA-approved,

generally accessible, well-reviewed in the literature, relatively less expensive, and perform for a sizable patient population on a daily basis, whereas this is not the case for the usage of PET compounds. Due to their capacity to image endogenous ligands like peptides and antibodies and their capacity to assess relatively slow kinetic processes as a result of the comparatively long half-lives of the typically utilized isotopes, SPECT radiotracers occupy a specific position in the molecular imaging matrix (in comparison to PET). Additionally, SPECT systems can simultaneously portray two chemical pathways by monitoring their associated photon emissions because to the capacity to assess two separate photon energies. In this chapter, we go over some fundamental ideas related to the manufacturing, generator, and qualities of radiopharmaceuticals utilized in clinical practice

Production of Radiopharmaceuticals

Due to their lengthy half-lives, naturally occurring radionuclides cannot be used for medical diagnostics, necessitating the creation of alternative radionuclides suitable for medical usage. The majority of radionuclides used in medicine are created in cyclotrons or nuclear reactors. Some radionuclides are extracted from generators where the parent radionuclide is created in a reactor or cyclotron.

Reactor Produced Radionuclides

The fission of the fissile material that makes up the fuel rods of a nuclear reactor (such as U235 or P239) is induced by neutrons, and the number of neutrons released in that fission process is approximately two or three neutrons with a mean energy of 1.5 MeV.

$$U235 + n = \text{fission products} + un$$

These fresh neutrons are then employed to cause fission in other nuclei, which releases fresh neutrons and starts the chain reaction. Neutron moderators (low molecular weight materials like water, heavy water, and graphite, which are distributed in the spaces between the fuel rods) and neutron absorbers (such as cadmium rods placed in the fuel core) are used to thermalize and reduce the energy of the emitted neutrons to 0.025 eV to maintain equilibrium in order to control this chain reaction and prevent a potential meltdown situation in the reactor. Thermal neutron reactions and fission (n, f) reactions are the two types of nuclear reactions that are employed to create radioisotopes that are

of interest from a medical standpoint.

Cyclotron Produced Radionuclides

A large variety of nuclear medicine radiopharmaceuticals are produced using cyclotron devices, which were first developed in 1930. This is especially true for radiopharmaceuticals with short half-lives. The fundamental idea behind how they work is to accelerate charged particles like protons, deuterons, and a-particles in a spiral path within two "dees," or semicircular, flat, evacuated metallic cylinders. The dees are positioned between a magnet's two poles, causing the ion beam to be restricted to a circular path inside the dees. The imposition of the potential difference causes the ions to accelerate at the gap between the dees. The beam particles start at the ion source in the cyclotron's center and spiral outward in the dees, gaining more energy with each trip across the dees gap. The high-energy particles eventually exit the dees and are directed toward the object of the bombardment. Because of the relativistic rise in mass of the accelerated particle, fixed-frequency cyclotrons can only accelerate positively charged ions up to 50 MeV for protons, whereas linear accelerators can accelerate particles up to several hundred mega-electron-volts due to their capacity to compensate for the mass increase of high-energy particles In order to use cyclotrons to accelerate particles to considerably greater energy, sophisticated techniques have been devised. Medical cyclotrons accelerate negatively charged ions, whereas the bulk of cyclotrons constructed before 1980 accelerate positively charged ions (i.e., H+) (H). With the help of a thin carbon foil that intercepts the beam and removes the negative ions at the end of its course, the design enables the creation of a straightforward deflection system that produces a positively charged H+ beam. Due to the magnetic field, the beam then changes direction without a deflector the H+ bombards the target in a manner akin to that of a cyclotron for positively charged ions. Additionally, the beam can be extracted from the machine at two distinct locations, enabling the employment of a negative-ion cyclotron for the simultaneous generation of two different radioisotopes. Usually, a nuclear reaction occurs when the accelerated particles irradiate the target nuclei. Depending on the input particle's energy, the nucleus may retain some of the incident particle's energy after the encounter or may totally absorb it. In either scenario, the nucleus is excited, causing nucleon (protons and neutrons) emission and then g-ray emission. Numerous nucleons may be randomly released from the irradiation nucleus, depending on the energy left over by the impact particle, resulting in the creation of various nuclides. More nucleons are emitted

as the irradiating particle's energy rises, which can lead to the production of a wider range of nuclides. The creation of 111In by bombarding 111Cd with 12-MeV protons is an illustration of a straightforward radionuclide created in a cyclotron. The following is an expression for the nuclear reaction:

111Cd (p, n)111In

Due to a lack of energy after the first neutron is emitted, a second nucleon may not be emitted in this scenario. G-ray emission will be used to discharge any excitation energy that is insufficient to continue emitting nucleons. To prevent the creation of extraneous radioisotopes, the target material must be pure and ideally monoisotopic, or at least enriched in the targeted isotope. As to inhibit the existence of undesirable radionuclides, the energy and type of the irradiating particle must be picked, as well.

Generator Produced Radionuclides

Early in the 1960s, Brookhaven National Laboratories built the first commercial radionuclide generator; since then, numerous new types of generators are developed for varied uses in nuclear medicine. Because of their capacity to continually produce a relatively short-lived daughter radionuclide, generators are defined as "parent daughter systems involving a long-lived parent radionuclide that decays to short half-life daughter." Chemical separation is feasible because the parent and its daughter nuclides are not isotopes. (13) Glass or plastic columns with a filtered disc attached to the bottom make up radionuclide generators. The parent nuclide is absorbed on the absorbent material, such as alumina, that is installed in the column. When a transient or secular equilibrium is attained, daughter radionuclides are produced by the parent radionuclide's decay, and they then appear to decay at the parent's half-life. As the daughter is not an isotope of the parent radionuclide, it must be eluted in a carrier-free state using a sterile and pyrogen-free solvent. As the daughter's activity increases up to equilibrium, several elution’s can be performed.

To get an eluted radionuclide that has been sterilized, various techniques can be used:

- The generator's whole column is autoclaved.
- Column preparation takes place in a generally aseptic space.
- The generator column is supplemented with bacteriostatic substances.

- The column's end has a membrane filter unit attached to it.
- Procedures for elution are carried out in an aseptic area.

Some Generator Systems Used in Nuclear Medicine Applications

Parent	Parent (T1/2)	Nuclear Reaction	Daughter	Daughter (T1/2)	Mode of Daughter decay	Principal keV	Eluant
Mo99	66h	Fission	Tc99	6h	IT	140(90)	0.9% NaCl
Y87	80h	Sr88(p,2n)	mSr87	2.8h	IT	388(82)	0.15M NaHCO3
Ge68	271 days	Ga69(p,2n)	Ga68	68 min	B+	511(178)	0.005M EDTA
Zn63	9.3 h	Cu63(p,2n)	Cu62	9.7 min	B+	511(194)	2N HCL
Sr82	25.5 days	Rb82 (p,2n)	Rb82	75s	B+	511(190)	0.9% NaCl

Molybdenum Generator

Since its initial commercial release in 1965, the 99Mo-99mTc generator has been the radionuclide generator most widely implemented in nuclear medicine. It has various enticing qualities and traits, which can be summed up as follows:

- Inexpensive and easy to use
- Devoid of pyrogens and sterile
- Radiochemical purity and high radionuclide levels
- Often utilized in nuclear medicine departments and used to manufacture a lot of Tc-99m labeled radiopharmaceuticals.
- The daughter nuclide's ideal half-life (6 h) and ideal energy (140 keV, 90% abundance)
- To produce a carrier-free 99Mo radionuclide, the (n, f) fission reaction was used instead of the (n, g) reaction. 99Mo has a half-life of 66 hours and decays by b-emission (87% to 99mTc) and in 13% to the ground state (99Tc), whereas 99mTc has a half-life of 6 hours and decays to 99Tc by an isomeric transition with it.

APPENDIX C. Curriculum Vitae

Personal Informations

Name	BURAK	**Surname**	AKGÜL

Education

Degree	Department	The name of the Institution Graduated From	Graduation year
Doctorate	NA	**NA**	NA
Master	NA	**NA**	NA
University	ESKİŞEHİR OSMANGAZİ ÜNİVERSİTESİ	**FEN-EDEBİYAT FAKÜLTESİ, FİZİK BÖLÜMÜ**	2008
High school	MUĞLA TURGUT REİS LİSESİ (YDA)	**SAYISAL**	2002

[#] All the grades must be listed if there is more than one (KPDS, ÜDS, TOEFL; EELTS vs),

Languages	**Grades ([#])**
ENGLISH	FLUENT

Work Experience (Sort from present to past)

Position	Institute	Duration (Year - Year)
MODALITY CLINICAL MANAGER – MOLECULAR IMAGING	GE HEALTHCARE – TURKEY	2011-
MI SERVICE REPRESENTATIVE	POZITRON LTD TURKEY	2010-2011
MI APPLICATION SPECIALIST	SIEMENS TURKEY	2008-2010

Computer Skills

Program	Level
Office (word, excel, power point)	Good
GE HEALTHCARE AW&XELERIS	Excellent

***Excellent , good, average or basic**

Scientific works

The articles published in the journals indexed by SCI, SSCI, AHCI

Articles published in other journals

Proceedings presented in international scientific meetings and published in proceedings book.

Journals in the proceedings book of the refereed conference / symposium

Others (Projects / Certificates / Rewards)